Dear Reviewer

First, we would like to thank you and the reviewers for your effort and the time spent to evaluate the manuscript entitled "**Ozone Downward Flux Revealed by High-Resolution Differential Absorption Lidar over Tibet during Stratosphere-Troposphere Exchange" (egusphere-2026-3261)**" We are sure that their valuable comments will improve the quality of our research work. We also would like to thank the editorial board for his guidance to proceed further. Following the reviewers' suggestions, we have revised this manuscript and highlighted the modifications in the revision. The point to point response to the comments are given below.

Response to Referee 1

We would like to thank the reviewer for the efforts and time and appreciate the encouraging review. Thank you for pointing out our mistakes. We really believe that your feedback has helped us to improve the presentation of our manuscript and the quality of our paper.

Following your suggestion, we have revised the organization of the manuscript and updated the relevant figures. We have also expanded the methodological discussion and incorporated additional relevant references to improve the clarity and completeness of the manuscript. The specific revisions are as follows:

General Remarks

The manuscript describes the observation and analysis of the short-term structures above a region with complex terrain. The description of the tropopause oscillations and the most likely underlying wave activity is neither really clear nor convincing. Models are used without demonstrating their capability of reproducing the observed tropopause structures. I cannot suggest publication in the current state.

Our Response:

Thank you for your careful assessment and constructive criticism. In response to the reviewer's concerns, we have substantially revised the observational analysis, dynamical interpretation, methodological description, and relevant figures.

First, we now separate the direct lidar observations from their subsequent physical interpretation. The features T0-T6 are described as short-lived downward-displacement episodes of ozone-enhanced structures rather than as individual downward-transport events. Whether these features are related to transport is assessed only after considering the temperature, PV, and flux diagnostics. The corresponding revisions are provided in Lines 208-234.

Second, we have strengthened the simultaneous ozone-temperature analysis, which is a central observational contribution of this study. The identification of T0-T6 is now described more clearly, and the temperature profiles independently retrieved from the simultaneously measured 387-nm N_2 Raman return are compared with the ozone structures on an event-by-event basis. Six of the seven episodes are associated with temperature gradients exceeding 8 K km^{-1}, while T2 exhibits a gradient of 4.2 K km^{-1}. We now present this as an observed co-temporal and co-altitudinal correspondence, rather than as independent proof of irreversible transport.

Third, we have clarified the distinction between the regional tropopause fold and the shorter-timescale oscillations identified by the reviewer. The fold is diagnosed from the regional PV structure over approximately 25-28°N and 95-99°E, where a downward intrusion of high-PV stratospheric air is evident and spatially coincides with enhanced cross-tropopause mass flux in Figs. 9 and 10. The shorter-timescale variations near the lidar site are interpreted as wave-related tropopause oscillations superimposed on this regional folding structure. These processes are not mutually exclusive: observational studies have shown that jet-associated tropopause folds can be accompanied by inertia–gravity waves, wave breaking, turbulence, and related instabilities (Cho et al., 1999; Bertin et al., 2001; Stohl et al., 2003). The corresponding clarification is provided in Lines 378-385.

Fourth, we have clarified the role of ERA5. ERA5 is an observation-assimilating reanalysis rather than an unconstrained theoretical model field (Hersbach et al., 2020). We do not expect it to reproduce every sub-hourly structure resolved by the lidar. Instead, the lidar provides local, high-spatiotemporal-resolution ozone and temperature observations, whereas ERA5 supplies the regional three-dimensional dynamical fields required to define the tropopause, characterize the PV structure, and diagnose cross-tropopause fluxes. Figure 5 demonstrates that ERA5 captures the overall onset and recovery of the event and agrees well with the lidar in the magnitude and temporal evolution of ozone near the tropopause.

Finally, we have strengthened the robustness of the flux diagnosis. The uncertainty associated with the dynamical-tropopause definition is now evaluated through a PV-threshold sensitivity analysis and an examination of PV-surface continuity. On this basis, 3 PVU is adopted as a physically reasonable and representative threshold for this event rather than as a uniquely correct value. In addition, because Eulerian diagnostics in pressure coordinates can suffer from numerical cancellation among large terms (Wirth, 1995; Wirth and Egger, 1999), Wei's formulation has been reformulated in PV coordinates. The recalculated results are presented in the revised Fig. 10, with the methodological explanation provided in Lines 392-400.

The revised interpretation is therefore supported by several complementary lines of evidence: high-resolution ozone observations, independently retrieved Raman-temperature profiles, regional PV morphology, PV-threshold sensitivity analysis, event-scale consistency between ERA5 and the lidar, and cross-tropopause mass- and ozone-flux calculations. We believe that these revisions have substantially improved the clarity and robustness of the manuscript and have addressed the reviewer's principal concerns regarding tropopause oscillations, wave activity, and the use of ERA5 data. We respectfully ask the reviewer to reconsider the manuscript in light of these revisions.

Specific Comments

Comments and Suggestions #1

Introduction: In the Introduction also the international literature on a topic should be reviewed.

Our Response:

We thank you for the careful evaluation of our work and for the valuable suggestions. We agree that the original Introduction focused mainly on studies over the Tibetan Plateau and did not sufficiently review the broader international literature on Stratosphere-Troposphere Exchange (STE).

We have therefore expanded the Introduction to include international studies on STE mechanisms and dynamical processes (Holton et al., 1995; Stohl et al., 2003), the global climatology of tropopause folds and cross-tropopause exchange (Sprenger et al., 2003; Škerlak et al., 2015), cross-tropopause mass and ozone fluxes (Olsen et al., 2004), and high-resolution ground-based ozone-lidar observations of stratospheric intrusions (Eisele et al., 1999; Kuang et al., 2012). These additions place the present study within a broader international context and provide a clearer transition to the remaining need for high-spatiotemporal-resolution observations over the Tibetan Plateau.

Changes in manuscript:

The corresponding additions are highlighted in yellow in the revised Introduction, particularly in Lines 29, 33, 35, 40, and 51. The relevant references have also been added or cited in the revised manuscript.

Comments and Suggestions #2

Lines 12-13: "It provides the first lidar-based detection of these rapid ozone descent events": I do not believe that you mean world-wide! There is a host of literature on this issue. Also "the evidence linking them to temperature variability in the tropopause region" is not new. You find this even in many radiosonde ascents

Our Response:

We thank you for the careful evaluation of our work and for the valuable suggestions.

In the revised manuscript, we have replaced the original statement, "It provides the first lidar-based detection of these rapid ozone descent events and the evidence linking them to temperature variability…"with the following more precise description: "The high-spatiotemporal-resolution lidar observations resolve a series of short-lived, rapid ozone descent episodes … including temperature gradients generally exceeding 8 K km^{-1}."

We have also more carefully defined the distinctive contribution of this study. we now emphasize three specific aspects: (1) the high-spatiotemporal-resolution characterization of the short-lived ozone descent episodes labelled T0-T6; (2) the event-by-event correspondence between these ozone features and rapid temperature variations near the tropopause, independently retrieved from the Raman signals measured by the same lidar system; and (3) the subsequent quantitative estimation of cross-tropopause ozone flux by combining the lidar-derived ozone profiles with the dynamical flux diagnosis.

Changes in manuscript:

The corresponding revision can be found in Lines 12-16 of the revised manuscript. These revisions clarify the scope of the observational contribution and avoid overstating the novelty of the study.

Comments and Suggestions #3

Line 27: STT has been studied since the 1950s. Why do you prefer to cite just Chen et al? I would expect a citation of least the last review paper of Stohl et al (JGR 2003) in addition.

Our Response:

Thank you for this important comment. We agree that citing only Chen et al. (2006) in this general statement did not adequately reflect the long history of research on stratosphere–troposphere exchange or the extensive international literature in this field. Following the reviewer's suggestion, we have added the comprehensive review by Stohl et al. (2003) at the corresponding location. We have also expanded the Introduction to provide a broader review of international STE research, including its major dynamical mechanisms and related observational studies.

Changes in manuscript:

The corresponding revision is highlighted in yellow in Lines 27-29 of the revised manuscript. The corresponding sentence has been revised as follows: "Stratosphere-troposphere exchange (STE) has been investigated for several decades and is recognized as a key process controlling the budgets of ozone, water vapor, and other trace constituents in the upper troposphere and lower stratosphere (UTLS) (Stohl et al., 2003; Chen et al., 2006)."

Comments and Suggestions #4

Lines 30-34: You could add a few words about the role of the subtropical jet stream in this context. Sprenger et al (JGR2003) found an STT maximum in that area.

Our Response:

Thank you for this helpful suggestion. We agree that the subtropical jet and its associated dynamical structures provide important context for understanding cross-tropopause transport over the Tibetan Plateau and surrounding regions. We have therefore added a brief discussion of the role of the subtropical jet to the revised Introduction. In particular, we now explain that the strong horizontal and vertical wind shear associated with the jet favors dynamical disturbances, tropopause deformation, and tropopause folding, with the latter providing an important pathway for cross-tropopause exchange.

We have also cited Sprenger et al. (2003) and added the following text: "The subtropical jet is particularly relevant in this context because its strong horizontal and vertical wind shear favors tropopause deformation and folding. Global analyses by Sprenger et al. (2003) showed ..."The study by Sprenger et al. (2003) demonstrated that tropopause folds occur preferentially in the subtropics and that a substantial fraction of cross-tropopause exchange events within the 20°-40° latitude band are associated with such folds.

Changes in manuscript:

The corresponding revisions are highlighted in yellow in Lines 36-40 of the revised manuscript.

Comments and Suggestions #5

Line 57: high resolution in time or in space?

Our Response:

Thank you for pointing out this ambiguity. Here, "high resolution" refers to both the temporal and spatial (vertical) sampling capabilities of the USTC Ozone Lidar. We have therefore revised the wording to "high-spatiotemporal-resolution observations" to make this point explicit.

During routine operation, the lidar records one raw signal profile every 1 min, with a vertical range-bin spacing of 61.44 m. For the stratospheric ozone retrievals used in this study, the photon-counting signals were accumulated over 30 min to ensure an adequate signal-to-noise ratio and were subsequently processed using a moving time-window method. Accordingly, the original expression "high-resolution observations" has been revised to "high-spatiotemporal-resolution observations."

Changes in manuscript:

The corresponding revision is highlighted in yellow in Lines 85-86 of the revised manuscript.

Comments and Suggestions #6

Section 2: The lidar specifications are missing.

Our Response:

We thank you for the careful evaluation of our work and for the valuable suggestions. The USTC Ozone Lidar used in this study is an established mobile differential absorption lidar (DIAL) system developed by our group. Its system configuration, technical specifications, and performance characterization have been described in detail in our previous instrumental paper (Fang et al., 2019). Because the focus of the present study is the application of this existing lidar system to the investigation and quantitative diagnosis of an STE-related ozone transport event, rather than the development or technical characterization of the lidar itself, we have avoided repeating the complete instrumental description provided in Fang et al. (2019).

Nevertheless, following the reviewer's suggestion, we have revised Section 2, particularly Lines 116-137, to provide a clearer summary of the key specifications directly relevant to the present observations. These include the transmitted and received wavelengths, telescope configuration and apertures, measurement altitude ranges, vertical range-bin spacing, and data-acquisition and accumulation intervals.

Changes in manuscript:

The key system specifications are provided in Lines 116-137, and the temporal and vertical sampling characteristics are described in Lines 144-148 and highlighted in green in the revised manuscript.

Comments and Suggestions #7

Lines 73-74: It is nice that you provide this capability. However, also lidar systems devoted to STT studies should be mentioned (e.g., Ancellet et al, Langford et al, Eisele et al, 1997, Kuang et al, Trickl et al, 2020).

Our Response:

We thank you for the careful evaluation of our work and for the valuable suggestions. We agree that the original description did not sufficiently acknowledge previous ozone lidar observations specifically devoted to stratosphere-to-troposphere transport (STT) and stratospheric intrusion studies. We have therefore expanded Section 2 to place the USTC Ozone Lidar observations in the context of these earlier international lidar studies.

In the revised manuscript, we now cite representative studies by Ancellet et al., Eisele et al., Langford et al., Kuang et al., and Trickl et al., which have demonstrated the capability of ground-based ozone lidar to resolve ozone-rich stratospheric intrusion layers and to investigate their descent, evolution, and mixing in the troposphere. These references provide a more complete context for the application of high-resolution ozone lidar observations to STT studies.

Changes in manuscript:

The following text has been added to Section 2(lines105-113): "Ground-based ozone lidar has also been extensively applied to studies of stratosphere-to-troposphere transport (STT) and stratospheric intrusions. Early studies demonstrated the capability of ozone lidar to resolve ozone-rich layers associated with cross-tropopause exchange and tropopause-folding events (Ancellet et al., 1991; Eisele et al., 1999). Subsequent lidar observations have been used to investigate the descent, evolution, and mixing of stratospheric ozone intrusions in the free troposphere (Langford et al., 2009; Kuang et al., 2012). More recently, long-term ozone lidar observations have further demonstrated the frequent occurrence and substantial influence of stratospheric intrusion layers in the free troposphere (Trickl et al., 2020)."

Comments and Suggestions #7

Lines 78-81: Although lidar details are not ultimately essential for this study, a few more words could be added. For instance, it should be briefly explained why so many wavelengths are required and how they are generated (including citations).

Our Response:

Thank you for this helpful suggestion. We agree that, although the detailed instrumental design is not the main focus of the present study, a brief explanation of the purpose and generation of the different wavelengths is useful for understanding the measurement strategy. We have therefore expanded Section 2 accordingly and added relevant references.

The different wavelength pairs are employed to accommodate the large difference in ozone abundance between the troposphere and stratosphere and the corresponding requirements for differential-absorption sensitivity and measurement range. For tropospheric ozone measurements, the 289/299-nm DIAL pair is used to provide sufficient differential ozone absorption sensitivity at relatively low ozone concentrations. These wavelengths are generated through stimulated Raman scattering by pumping D_2 and H_2 Raman cells, respectively, with 266-nm radiation obtained from the fourth harmonic of a Nd laser (Papayannis et al., 1999; Fang et al., 2019). For stratospheric ozone measurements, where ozone abundance is substantially higher, the 308/355-nm DIAL pair is employed. The 308-nm wavelength is generated directly by a XeCl excimer laser, while the 355-nm wavelength is obtained through third-harmonic generation of the 1064-nm fundamental output of a Nd laser (McDermid et al., 1991; Godin-Beekmann et al., 2003; Fang et al., 2019). In addition, the N_2 vibrational Raman returns at 332 and 387 nm, corresponding to excitation at 308 and 355 nm, respectively, are simultaneously detected (McGee et al., 1993) to reduce aerosol/backscatter-related effects.

Changes in manuscript:

We have incorporated the above explanation and the corresponding references into Section 2 of the revised manuscript. The relevant revisions are highlighted in yellow in Lines 116-130.

Comments and Suggestions #8

Line 79: This wavelength pair does not allow for good vertical resolution unless there is a very strong ozone peak.

Our Response:

Thank you for your careful evaluation of our study and for your valuable suggestion. In the original manuscript, we stated that the USTC Ozone Lidar uses 289/299 nm for tropospheric measurements and 308/355 nm for stratospheric measurements.

Because ozone abundance differs significantly between the troposphere and the stratosphere, the USTC Ozone Lidar uses different wavelength pairs for measurements in these two altitude regions. For the troposphere, where the ozone number density is relatively low, the system uses the 289/299-nm DIAL wavelength pair (Papayannis et al., 1999; Kourtidis et al., 2002; Fang et al., 2019). The sufficiently large absorption cross sections at these wavelengths, together with the sufficiently large difference in absorption cross section resulting from the 10 nm wavelength separation, ensure adequate differential-absorption sensitivity. To maintain good signal quality over a relatively broad measurement range, the system employs two receiving configurations: a low-altitude channel covering approximately 5-10 km and a high-altitude channel covering approximately 8-19 km.

For stratospheric measurements, where ozone abundance is significantly higher, the system uses the 308/355-nm wavelength pair (McDermid et al., 1991; Godin-Beekmann et al., 2003), which enables the ozone-profile measurement range to be extended to higher altitudes. In addition, the system simultaneously detects the 332 nm and 387 nm nitrogen (N_2) vibrational Raman scattering signals generated by excitation with the 308 nm and 355 nm lasers, respectively (McGee et al., 1993). These Raman channels provide complementary information, helping to reduce the effects of aerosols and backscatter during the ozone retrieval and to improve the reliability of the measurements, particularly in the upper-tropospheric and stratospheric regions.

Changes in manuscript:

The corresponding explanation has been added to Lines 116-130 of the revised manuscript and is highlighted in yellow.

Comments and Suggestions #9

Line 83: Please, add a reference such as (McGee et al, 1993).

Our Response:

Thank you for this helpful suggestion. We agree that a reference to the established Raman lidar technique is appropriate here. Following the reviewer's suggestion, we have cited McGee et al. (1993) in the corresponding description of the N_2 Raman backscatter measurements in Section 2, and the full citation has been added to the reference list.

Changes in manuscript:

The corresponding revision can be found in Line 128 of the revised manuscript.

Comments and Suggestions #10

Line 88: Are the heights specified above the ground or above sea level?

Our Response:

Thank you for pointing out this ambiguity. The heights reported here are measured above sea level, rather than above mean ground level. We have clarified this in Section 2 by explicitly specifying "above sea level" for the corresponding height ranges.

Changes in manuscript:

The corresponding revisions can be found in Lines 134-138 of the revised manuscript.

Comments and Suggestions #11

Line 110: Please, cite the appropriate chapter in that book. This chapter, however, does not fully describe the state of the art of ozone lidar systems. What about aerosol and cloud interference? What about lidar calibration and uncertainty? References are needed.

Our Response:

We thank you for the careful evaluation of our work and for the valuable suggestions. We agree that the description in the original manuscript was too brief and that the general citation to Weitkamp (2005) did not adequately address the retrieval issues specific to ozone DIAL measurements. We have therefore substantially revised the corresponding part of Section 2 and added more targeted references.

First, following the reviewer's suggestion, we now cite the specific chapter by Gimmestad (2005), entitled "Differential-Absorption Lidar for Ozone and Industrial Emissions," rather than referring only to the book as a whole. We have also clarified the major factors considered in the ozone retrieval, including the temperature dependence of the ozone absorption cross-sections, absorption by interfering atmospheric species, and the wavelength dependence of molecular and aerosol backscatter and extinction.

Second, we have expanded the discussion of aerosol and cloud interference. Differences in aerosol backscatter and extinction between the online and offline wavelengths can introduce systematic errors, particularly when strong vertical gradients in aerosol loading are present. We have therefore added ozone-DIAL-specific references addressing these effects (Browell et al., 1985; Kovalev and Bristow, 1996). We further explain that the N_2 vibrational Raman returns at 332 and 387 nm provide complementary information that helps reduce aerosol- and backscatter-related effects in upper-tropospheric and stratospheric ozone retrievals.

Finally, we have clarified the treatment of system characterization, retrieval uncertainty, and validation. The detailed system characterization, retrieval methodology, and uncertainty assessment of the USTC Ozone Lidar have been presented in our previous instrumental study, Fang et al. (2019). For the measurements used in the present study, the retrieved ozone profiles are further evaluated through comparisons with ERA5 and independent Aura/OMI and Aura/MLS observations, as shown in Fig. 3. We emphasize that these comparisons provide independent validation of the retrieved ozone profiles rather than serving as an absolute instrumental calibration.

Changes in manuscript:

The above discussion and the corresponding references have been added to Section 2 of the revised manuscript, particularly Lines 153-165.

Comments and Suggestions #12

Line 115: Please, add citations for the satellites.

Our Response:

Thank you for this helpful suggestion. We have added appropriate references for the Aura satellite mission and for the satellite instruments and ozone-profile products used in this study. Specifically, Schoeberl et al. (2006) is now cited for the EOS Aura mission, Liu et al. (2010) for the OMI ozone-profile retrievals, and Waters et al. (2006) for the Aura MLS instrument.

Changes in manuscript:

The corresponding revision can be found in Lines 170-171 of the revised manuscript. The corresponding sentence has been revised as follows: "The merged profile was then compared with ERA5 data for the corresponding time and further cross-validated against ozone-profile observations from the Ozone Monitoring Instrument (OMI; Liu et al., 2010) and the Microwave Limb Sounder (MLS; Waters et al., 2006) aboard the Aura satellite (Schoeberl et al., 2006), as shown in Fig. 3(b)."

Comments and Suggestions #12

Line 128: How fine?

Our Response:

Thank you for pointing out that the term "fine-scale" was too qualitative. We have revised the corresponding text to provide a quantitative description based on the temporal scales actually resolved in our observations. Specifically, during this event, the USTC Ozone Lidar resolved short-lived downward-displacement episodes of ozone-enhanced structures occurring on sub-hourly to 1-2 h timescales, as further presented and discussed in Section 3.1.

The corresponding text has been revised as follows: "Moreover, the high spatiotemporal sampling capability of the lidar allows it to resolve vertically confined and short-lived ozone structures that are often missed by other datasets, since satellite profile data typically contain only about a dozen vertical points and ERA5 records only slightly more than 30 pressure levels. In particular, the lidar observations resolve short-lived ozone descent structures occurring on sub-hourly (approximately 30 min) to 1-2 h, as discussed in Section 3.1. This capability is particularly valuable for detecting and analyzing transient cross-tropopause ozone transport events."

Changes in manuscript:

The corresponding revisions are highlighted in yellow in Lines 183-187 of the revised manuscript.

Comments and Suggestions #13

Figure 3: An explanation of the inserts RAYLEIGH, RAMAN and MIE/RAYLEIGH is missing in the caption.

Our Response:

Thank you for pointing this out. We agree that the labels "RAYLEIGH," "RAMAN," and "MIE/RAYLEIGH" in Fig. 3(a) were not adequately explained in the original caption. We have therefore revised the caption to define these labels and clarify the backscatter-detection schemes and wavelength channels associated with the different ozone-profile segments.

Specifically, "MIE/RAYLEIGH" denotes the elastic Mie and Rayleigh backscatter signals at 289 and 299 nm used for the tropospheric ozone measurements; "RAYLEIGH" denotes the elastic Rayleigh backscatter signals at 308 and 355 nm used for the stratospheric ozone measurements; and "RAMAN" denotes the N_2 vibrational Raman backscatter signals at 332 and 387 nm, corresponding to excitation at 308 and 355 nm, respectively. The associated wavelengths have also been specified in the revised figure caption.

Changes in manuscript:

The corresponding revisions can be found in Lines 190-194 of the revised manuscript.

Comments and Suggestions #14

Lines 160-161: What justifies to name these ozone features as representing downward transport? With one exception I see just modulations of the tropopause. At this point I would just describe the observations and then relate them to the analysis if this really yields a proof of vertical transport and not just tropopause dynamics (which would be interesting as well).

Our Response:

Thank you for this important comment. We would first like to clarify that our interpretation of STE refers to the overall ozone episode spanning 18-19 October, rather than to each individual short-lived feature. The blue and orange arrows indicate the downward evolution and subsequent recovery of the ozone-enhanced structure, respectively. Considering the duration and vertical extent of this episode, together with the dynamical and flux evidence presented later in the manuscript, we interpret the overall event as an STE/STT event. No comparable episode was identified in the other available lidar observations during that month.

Nevertheless, we agree that the original manuscript interpreted the lidar-observed ozone features as downward transport too early in the analysis. A downward displacement of an ozone-enhanced structure in a time-height cross-section alone is not sufficient to demonstrate irreversible cross-tropopause transport, because such an apparent displacement may also result from temporal variations or undulations of the tropopause.

Following the reviewer's suggestion, we have revised Section 3.1 to distinguish clearly between the direct lidar observations and their subsequent dynamical interpretation. In the revised manuscript, we first describe the evolution of the ozone field in Fig. 4 strictly in observational terms. Specifically, the ozone-enhanced structure on 18 October is described as exhibiting a downward displacement in the time–height cross-section, whereas the structure on 19 October exhibits an overall upward displacement. Similarly, the short-lived features T0-T6 are now described as "short-lived downward-displacement episodes of ozone-enhanced structures" rather than as individual "downward-transport events."

We have also explicitly stated that, at this stage of the analysis, these features are interpreted only as vertical displacements of ozone-rich structures near the tropopause. Whether they represent irreversible cross-tropopause transport or primarily reflect displacement or undulation of the tropopause is subsequently assessed using the dynamical and flux diagnostics presented later in the manuscript. Accordingly, our interpretation of the overall event as stratosphere-to-troposphere transport is not based solely on the apparent downward displacement in the lidar observations. It is supported by the combined analysis of the ERA5 meteorological fields, tropopause evolution, Wei cross-tropopause mass-flux diagnosis, the spatial relationship between the diagnosed mass flux and tropopause folding, and the estimated cross-tropopause ozone flux. We therefore no longer treat each individual T0-T6 feature as direct evidence of irreversible vertical transport.

We thank the reviewer for this suggestion, which helped us distinguish more clearly between the directly observed ozone variability and its subsequent dynamical interpretation.

Changes in manuscript:

The corresponding revisions are highlighted in yellow in Lines 208-228 of the revised manuscript.

Comments and Suggestions #15

Fig. 4: Please, explain the arrows.

Our Response:

Thank you for pointing this out. Although the meanings of the arrows were described in the corresponding discussion in Section 3.1, we agree that the figure caption should be self-contained. The blue arrow in Fig. 4(a) indicates the observed downward displacement of the ozone-enhanced structure on 18 October, whereas the orange arrow in Fig. 4(b) indicates the overall upward displacement of the ozone-enhanced structure during its subsequent evolution on 19 October.

Changes in manuscript:

We have added an explicit explanation of both arrows to the caption of Fig. 4. The corresponding revisions can be found in Lines 221-224 of the revised manuscript.

Comments and Suggestions #16

Line 164: "Previous studies have given limited attention to such events." This remark is important! It also would also be valid for features e.g. caused by tropopause oscillations.

Our Response:

Thank you for this insightful comment. We agree that, in the original manuscript, the term "such events" could be interpreted too narrowly as referring specifically to short-lived downward-transport events. As noted in our response to the preceding comment, the lidar observations alone do not establish that each of the T0-T6 features represents irreversible cross-tropopause transport.

We have therefore revised this discussion to refer more generally to short-lived ozone structures near the tropopause and to explicitly acknowledge that rapid tropopause oscillations or undulations can also produce apparent vertical displacements of ozone-rich layers. We agree with the reviewer that these short-timescale features are scientifically relevant regardless of whether they ultimately reflect irreversible transport, tropopause dynamics, or a combination of the two.

The revised text reads: "Previous studies have given comparatively limited attention to such short-lived ozone structures near the tropopause. Importantly, these features should not necessarily be interpreted as individual cross-tropopause transport events, since rapid tropopause oscillations or undulations may also produce apparent vertical displacements of ozone-rich layers. Their repeated occurrence on sub-hourly to hourly timescales nevertheless provides a useful observational perspective on fine-scale ozone variability and tropopause dynamics. The relationship of these features to tropopause variability and cross-tropopause transport is examined further using the temperature, dynamical, and flux diagnostics presented below."

Changes in manuscript:

The corresponding revisions can be found in Lines 228-234 of the revised manuscript.

Comments and Suggestions #17

Line 253: USSA1976 model

Line 253: Please, specify USS1976 and add a reference.

Our Response:

Thank you for pointing this out. In the revised manuscript, we have clarified both the full name and the role of USSA1976 in the temperature-retrieval procedure. Specifically, USSA1976 refers to the U.S. Standard Atmosphere 1976. The temperature specified by this standard atmosphere at 50 km was adopted as the upper-boundary reference for the Raman temperature retrieval, and the temperature profile was subsequently retrieved downward from this reference altitude. The corresponding reference to the U.S. Standard Atmosphere 1976 has also been added to the reference list.

Changes in manuscript:

The revised text reads: "The temperature retrieval, shown in Fig. 8(b), was initialized at 50 km using the temperature from the U.S. Standard Atmosphere 1976 as the upper-boundary reference (U.S. Standard Atmosphere, 1976), and the temperature profile was subsequently retrieved downward from this reference altitude." The corresponding revision can be found in Lines 343-345 of the revised manuscript.

Comments and Suggestions #18

Figs. 9 and 10: What does the red asterisk mean? Please, add information on the method to the caption.

Our Response:

Thank you for pointing this out. The meaning of the red symbol and the method used to calculate the cross-tropopause mass flux were already described in the main text, but we agree that this information should also be included in the figure captions so that the figures can be interpreted independently.

We have therefore revised the captions of Figs. 9 and 10 to clarify that the red asterisk marks the location of the USTC Ozone Lidar at Yangbajing (29°N, 99°E). We have also added that the cross-tropopause mass fluxes were diagnosed using Wei's formulation together with ERA5 meteorological fields, and that the displayed fields represent 6-h means of the instantaneous mass flux over the corresponding time intervals. For Fig. 9, the individual contributions from tropopause motion, horizontal advection, and vertical motion, as well as the total mass flux, are now explicitly identified in the caption.

Changes in manuscript:

The corresponding revision can be found in Lines 387-389 and 433-435 of the revised manuscript.

Comments and Suggestions #19

Line 209: How did you determine the temperature lapse rate for all times?

Our Response:

Thank you for this question. We apologize that the calculation procedure was not described sufficiently clearly in the original manuscript. In this study, the temperature lapse rate and the corresponding thermodynamic tropopause were determined independently at each available ERA5 time step, rather than deriving them from a single time and extrapolating the results to other times.

Specifically, for each ERA5 time step, the temperature lapse rate was calculated from the corresponding vertical temperature profile, after which the WMO lapse-rate criterion was applied to identify the thermodynamic tropopause.

Changes in manuscript:

We have clarified this calculation procedure in Lines 241-245 of the revised manuscript.

Comments and Suggestions #19

Line 220: PV is derived from model analyses. How can you expect that the models match your rather detailed observations? See line 248.

Our Response:

We thank you for the careful evaluation of our work and for the valuable suggestions. We agree that, because of the substantial difference in spatial and temporal resolution, the ERA5-derived potential-vorticity (PV) fields cannot be expected to reproduce the short-lived, fine-scale ozone structures resolved by the lidar. It was not our intention to imply a point-by-point or event-by-event correspondence between the ERA5 PV fields and the individual lidar-observed features. We have clarified this point in the revised manuscript.

In this study, the ERA5-derived PV fields and the lidar observations serve different but complementary purposes. The lidar provides local, high-spatiotemporal-resolution observations of the evolution of ozone structures near the tropopause. In contrast, the ERA5-derived PV fields provide an observation-constrained and dynamically consistent description of the regional-scale atmospheric environment. They are used to define the dynamical tropopause, characterize the broader dynamical evolution of the STE event, and provide the framework required for the subsequent cross-tropopause mass-flux diagnosis. Accordingly, the PV-threshold analysis in Section 3.2 is intended to identify a physically reasonable dynamical-tropopause definition for the regional flux calculation, rather than to reproduce the individual short-lived features T0-T6 observed by the lidar.

This distinction is also consistent with the discussion around Line 248 of the original manuscript. The hourly ERA5 fields are suitable for characterizing the event-scale evolution of the tropopause, the regional tropopause-folding structure, and the associated cross-tropopause transport during this approximately one-day STE event. They cannot, however, resolve all of the sub-hourly to hourly variability detected by the lidar. For this reason, the individual short-lived ozone features are not interpreted solely on the basis of the ERA5-derived PV fields. Instead, their detailed temporal evolution is examined independently using the high-resolution lidar observations, including the temperature profiles retrieved from the simultaneously measured 387-nm N_2 vibrational Raman return. For the reviewer's reference, we show below the diagnosed cross-tropopause mass-flux field for 17 October. This figure is provided only in the present response and has not been added to the revised manuscript. Before the event observed on 18-19 October, neither the ERA5-based flux diagnosis nor the available lidar observations indicated pronounced cross-tropopause activity. In contrast, from 18 October onward, both datasets captured the onset and evolution of the STE event illustrated in Fig. 4. Thus, the ERA5-based diagnosis and the lidar observations consistently identify the occurrence and overall timing of the event at the event scale, while the lidar additionally resolves the finer vertical and temporal structures embedded within the event.

Our analysis therefore considers two complementary spatial and temporal scales. ERA5/PV provides the regional dynamical framework and the cross-tropopause flux diagnosis used to identify and interpret the overall STE/STT event, whereas the lidar resolves the local fine-scale ozone and temperature variability embedded within that larger-scale event. We have revised the manuscript to make this distinction explicit and to avoid suggesting that the ERA5-derived PV fields should reproduce the detailed lidar observations.

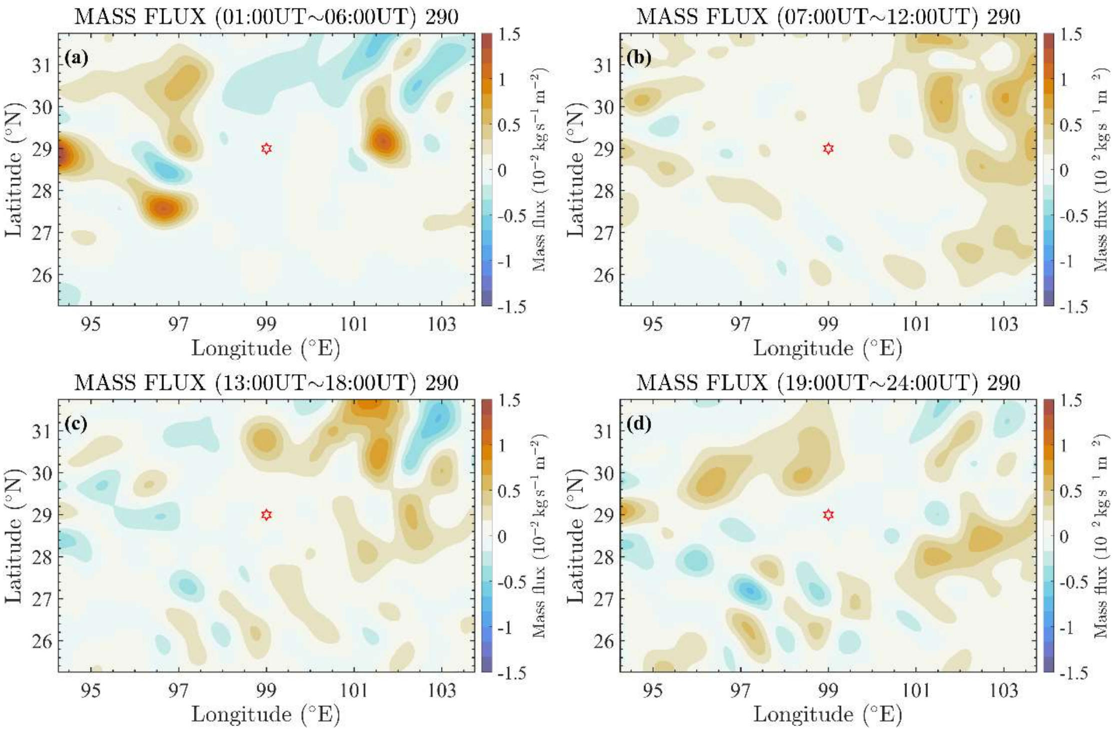

Figure.response19: The diagnosed cross-tropopause mass-flux field for 17 October

Changes in manuscript:

The corresponding revisions can be found in Lines 291-298 and 336-339 of the revised manuscript.

Comments and Suggestions #20

Fig. 7: Consider moving the data to line 1 of the caption since it seems to be representative for all panels.

Our Response:

Thank you for this suggestion. We agree that the date applies to the figure as a whole and is more appropriately stated at the beginning of the caption. We have therefore moved the date to the first line of the Fig. 7 caption and revised the descriptions of the individual panels accordingly.

Changes in manuscript:

The corresponding revision can be found in Lines 321-324 of the revised manuscript.

Comments and Suggestions #21

Lines 242-243: How accurate is this theoretical wind field? Does it represent the observations?

Our Response:

Thank you for this important comment. We would like to clarify that the wind fields used in this study were obtained from the ERA5 reanalysis rather than from a purely theoretical model. Because the lidar system did not provide simultaneous real-time wind measurements during the observation period, ERA5 served as an appropriate alternative source of wind information for the present analysis. ERA5 assimilates a wide range of atmospheric observations and provides observation-constrained, dynamically consistent three-dimensional meteorological fields (Hersbach et al., 2020). In the present study, the ERA5 wind fields are used at the regional dynamical scale to characterize the atmospheric circulation and to provide the horizontal and vertical wind components required for Wei's cross-tropopause mass-flux diagnostic. We neither expect nor require the ERA5 fields to reproduce every short-lived, fine-scale structure resolved by the lidar. Rather, the two datasets serve complementary purposes: the lidar provides local observations of ozone variability at high spatial and temporal resolution, whereas ERA5 supplies the observation-constrained three-dimensional dynamical fields required for the regional-scale analyses of the tropopause structure and cross-tropopause fluxes.

Figure 5 shows that ERA5 captures the overall onset and recovery of the event and agrees well with the lidar in the magnitude and temporal evolution of ozone near the tropopause. Although this does not directly validate the ERA5 wind fields, it supports the applicability of ERA5 to the event-scale analysis.

Changes in manuscript:

We have revised the corresponding text to clarify the nature and specific role of the ERA5 wind fields in the present analysis. The relevant revisions can be found in Lines 326-330 of the revised manuscript.

Comments and Suggestions #22

Lines 278-279: Again: How accurate is the tropopause?

Our Response:

Thank you for raising this important point again. The dynamical tropopause is a diagnostically defined transition surface rather than a directly observed boundary with a uniquely determined geometric height. Its diagnosed position depends on the selected PV threshold and the spatial resolution and structure of the meteorological fields. Therefore, an absolute vertical accuracy cannot be assigned from the available observations.

To evaluate this uncertainty, we explicitly tested the sensitivity of the diagnosed cross-tropopause transport to a range of commonly used PV thresholds. As shown in Fig. 6, lower thresholds produce larger upward and downward fluxes, whereas higher thresholds produce substantially smaller fluxes. We further examined the spatial continuity of the corresponding PV surfaces in the zonal and meridional cross-sections in Fig. 7(a-b). The lower-PVU surfaces are discontinuous in some regions,

while their continuity and stability improve markedly for thresholds of 2 PVU and above.
Based on both the flux-sensitivity results and the spatial continuity of the PV surfaces, we adopted 3 PVU as a physically reasonable and representative dynamical-tropopause threshold for this event, rather than as a universally optimal or uniquely defined value. The uncertainty associated with the tropopause definition is therefore addressed through the PV-threshold sensitivity analysis.

Changes in manuscript:

The corresponding clarification can be found in Lines 315-319 of the revised manuscript.

Comments and Suggestions #23

Line 286: I do not see the typical picture of a tropopause fold; please, explain.
Line 298 (and the following lines): I do not see “tropopause folding”, but an oscillating tropopause. In lines 307 and 308 a wave activity is mentioned!

Our Response:

Thank you for these important comments. We would, however, like to clarify that these two phenomena are not mutually exclusive. In a strongly sheared jet-front environment, a regional tropopause fold can coexist with, and be locally modulated by, inertia-gravity waves and associated tropopause oscillations. Thus, the presence of an oscillating tropopause or wave activity does not, by itself, exclude the existence of a regional tropopause fold.

Our identification of the fold is based primarily on the regional potential-vorticity (PV) structure rather than on the short-period oscillations observed near the lidar site. Over approximately 25-28°N and 95-99°E, the regional PV field exhibits pronounced deformation of the dynamical tropopause and a downward intrusion of high-PV stratospheric air toward the troposphere. The corresponding high-PV intrusion can also be identified in the zonal PV cross-section near 26°N in Fig. 7. Moreover, the spatial extent of this structure is consistent with the region of enhanced cross-tropopause mass flux diagnosed in Figs. 9 and 10. Therefore, the basis for identifying a regional tropopause-folding system is the combination of the downward-reaching high-PV structure and the dynamically consistent cross-tropopause flux, rather than the short-period oscillations of a single tropopause contour.

To strengthen the robustness of the flux diagnosis, we also revised the numerical implementation of Wei’s formulation. Eulerian diagnostics applied directly in pressure coordinates can be affected by numerical cancellation among individually large terms, potentially introducing substantial uncertainty into cross-tropopause flux estimates (Wirth, 1995; Wirth and Egger, 1999). Lagrangian trajectory-based approaches provide an alternative that is generally less susceptible to this cancellation problem and has been widely applied in global and large-domain studies of cross-tropopause transport (e.g., Wernli and Bourqui, 2002; Škerlak et al., 2014). For the present event-based regional analysis, however, we retained Wei’s diagnostic framework because it allows the flux to be explicitly decomposed into contributions from tropopause motion, horizontal advection, and vertical motion. Rather than applying the formulation directly in pressure coordinates, we transformed it into potential-vorticity coordinates and performed the calculation within the PV-coordinate framework. The revised results are presented in Fig. 10. Although this transformation does not eliminate all sources of uncertainty, it reduces the numerical sensitivity and part of the noise associated with cancellation among large terms. The corresponding methodological clarification is provided in Lines 392-400 of the revised manuscript.

We agree with the reviewer that pronounced tropopause oscillations are also present. These oscillations occur on shorter spatial and temporal scales and can be superimposed on the larger-scale folding structure. This interpretation is supported by previous observational studies showing that tropopause folds in strongly sheared jet-front environments can be accompanied by inertia-gravity waves, wave breaking, turbulence, and related dynamical instabilities. Cho et al. (1999), for example, directly observed gravity-wave breaking and dynamical instabilities within tropopause folds and showed that these processes can contribute to irreversible stratosphere-troposphere exchange. Similarly, Bertin et al. (2001), using a combined network of ST radars, temperature lidar, and ozone lidar, observed turbulent and stability structures during a tropopause-folding event that were consistent with unstable inertia-gravity waves generated in the jet-stream environment. The broader STE literature also recognizes tropopause folding and wave breaking as dynamically related processes that can jointly contribute to cross-tropopause exchange (Stohl et al., 2003).

Accordingly, the wave activity discussed later in the manuscript is not intended as an alternative explanation that rules out tropopause folding. Our interpretation is that the regional tropopause-folding system provides the larger-scale dynamical background, whereas gravity-wave activity produces shorter-timescale oscillations and local deformation of the tropopause and may further promote mixing and exchange. In other words, the regional high-PV intrusion is interpreted as the folding structure, while the oscillating tropopause noted by the reviewer represents shorter-scale wave-related modulation superimposed on that structure.

We have revised the manuscript to make this scale distinction and the diagnostic basis of the fold interpretation more explicit. The regional PV signature used to identify the fold and its relationship to the diagnosed mass flux are now described more clearly, while the shorter-timescale variations near the lidar site are characterized as wave-related tropopause oscillations superimposed on the evolving regional folding system. Relevant references have also been added to support this interpretation (Cho et al., 1999; Bertin et al., 2001; Stohl et al., 2003).

Changes in manuscript：

The corresponding revisions can be found in Lines 378-385 and 392-400 of the revised manuscript. The updated Fig. 10, recalculated using Wei’s diagnostic reformulated in potential-vorticity (PV) coordinates, is presented below for reference.

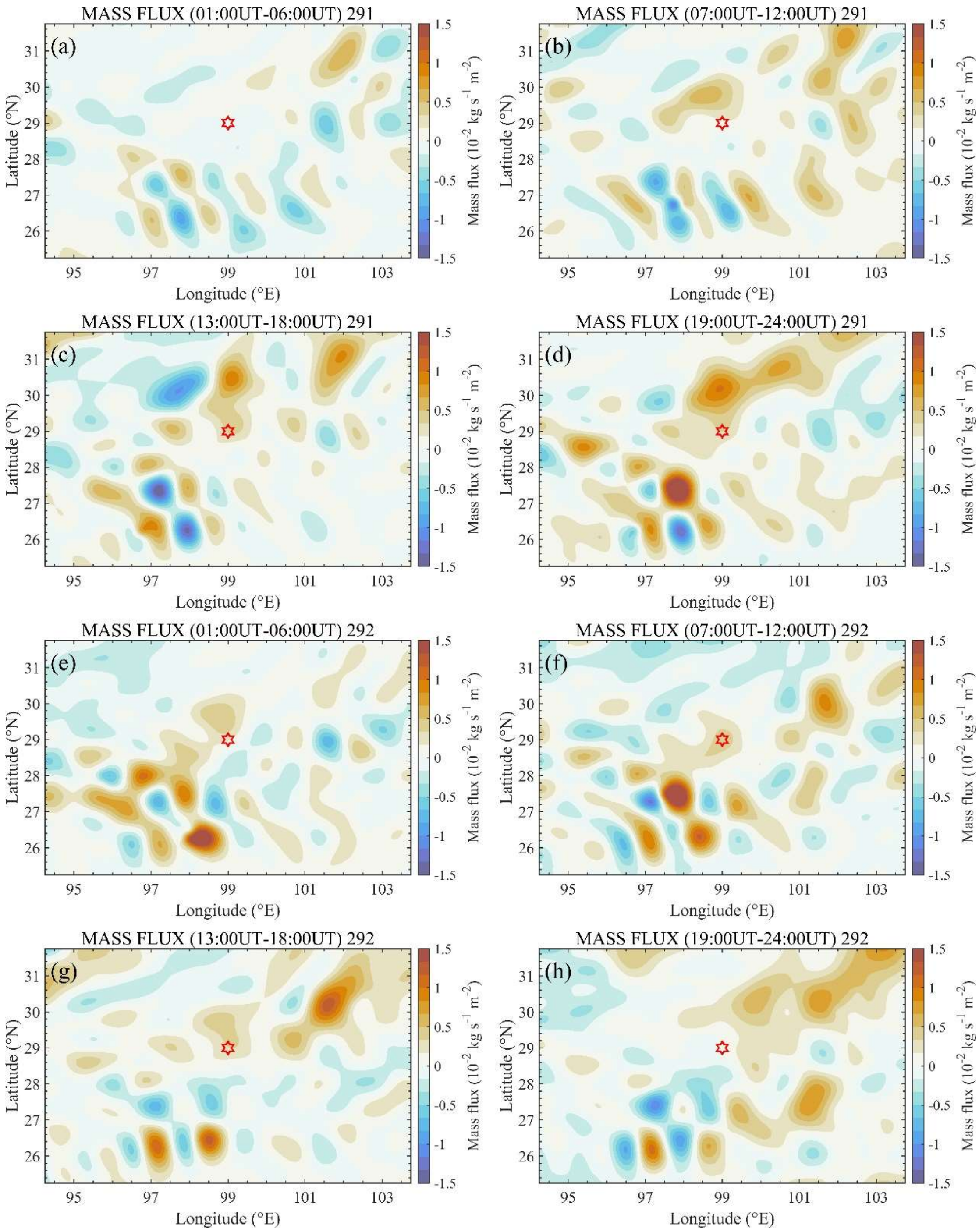

Figure 10: Spatiotemporal evolution of the cross-tropopause mass flux during 18-19 October 2017, diagnosed using Wei's formulation and ERA5 meteorological fields. Each panel shows the 6-h mean of the instantaneous cross-tropopause mass flux for the corresponding time interval. The red asterisk marks the location of the USTC Ozone Lidar at Yangbajing (29°N, 99°E).

Comments and Suggestions #24

Lines 328-331: Does this include the non-zero ozone-density gradients in the measured profiles?

Our Response:

Thank you for this question. We recognize that the term "uniform mixing ratio" used in the original description of Eq. (3) was misleading and could incorrectly suggest that ozone was assumed to be vertically constant within each layer.

In the actual calculation, $q(p)$ represents the pressure-dependent ozone mixing ratio derived from the lidar-measured ozone number-density profile, rather than a vertically uniform value. The complete $q(p)$ profiles within the 3-km layers immediately below and above the tropopause are integrated separately and normalized by their respective pressure intervals to obtain representative layer-mean ozone mixing ratios. Consequently, the observed vertical variability of ozone within each layer, including the effects of non-zero ozone gradients, is retained in the calculated layer means and therefore influences the resulting ozone-flux estimates.

To be precise, Eq. (3) does not contain a separate ozone-gradient term; instead, the effect of the measured vertical gradient is incorporated through the integration of the full pressure-dependent ozone profile. We have revised the explanation of Eq. (3) accordingly and removed the misleading expression "uniform mixing ratio."

Changes in manuscript:

The corresponding revisions can be found in Lines 438-453 of the revised manuscript.

Style

Comments and Suggestions #25

Line 20: what does the tilde mean? Consider revising. See also Figs. 7, 9 and 10.

Our Response:

We thank you for the careful evaluation of our work and for the valuable suggestions. The tilde symbol (~) was intended to indicate a numerical range rather than an approximation. We agree that this notation is ambiguous and have therefore replaced it with an en dash throughout the manuscript. For example, the ozone-flux value previously written as "3~4 × 10^{-10} kg s^{-1} m^{-2}" is now expressed as "(3-4) × 10^{-10} kg s^{-1} m^{-2}."

Changes in manuscript:

We have also checked and revised the corresponding notation in Figs. 7, 9, and 10 to ensure consistency.

Comments and Suggestions #26

Line 75: Again: what does the tilde mean? It is the mathematical symbol for "proportional to" and should not used here.

Our Response:

Thank you for pointing this out. Thank you for pointing this out. The tilde symbol (~) was used in the original manuscript to indicate "approximately" or, in some cases, a numerical range. We agree that this notation is potentially ambiguous and is not appropriate in this context. We have therefore removed the tilde notation throughout the manuscript.

Changes in manuscript:

Where an approximate value is intended, the symbol has been replaced by the word "approximately" (e.g., "approximately 4,300 m above sea level"). Where a numerical range is intended, the tilde has been replaced. We have also checked the corresponding notation in the figures and captions and revised it consistently.

Comments and Suggestions #27

Line 200: "Jacobian" is not precise. Please, extend.

Our Response:

We thank you for the careful evaluation of our work and for the valuable suggestions. We agree that referring to J_η simply as the "Jacobian" was not sufficiently precise. We have revised the corresponding definition to clarify that $J_\eta = \partial z/\partial \eta$ represents the vertical coordinate-transformation factor relating the generalized vertical coordinate η to geometric height z. This revision makes both the mathematical meaning and the role of J_η in the flux formulation more explicit.

Changes in manuscript:

The corresponding clarification can be found in Lines 272-273 of the revised manuscript.

Comments and Suggestions #28

Line 330: , thereby, Lines 274, 298. 383: , therefore, Line 393: ,but

Our Response:

Thank you for pointing out these punctuation and sentence-structure issues. We have revised the indicated sentences to remove or rephrase the constructions involving "thereby," "therefore," and "but," and have adjusted the punctuation and sentence structure where appropriate to improve grammatical accuracy, clarity, and readability.

Changes in manuscript:

The corresponding revisions can be found in Lines 365-366, 404-405, 438-440, 494-496, and 504-506 of the revised manuscript.

Response to Referee 2

We would like to thank the reviewer for the efforts and time and appreciate the encouraging review. Thank you for pointing out our mistakes. We really believe that your feedback has helped us to improve the presentation of our manuscript and the quality of our paper.

General Remarks

The topic of this manuscript is both necessary and scientifically meaningful for research on stratosphere-troposphere exchange over the Tibetan Plateau. The observational dataset used in this study is relatively rare. In particular, the lidar system employs four differential absorption wavelengths together with two nitrogen Raman channels, allowing simultaneous measurements of tropospheric and stratospheric ozone profiles as well as temperature profiles over the Tibetan Plateau. This dataset therefore has considerable scientific value. The short-duration and rapid ozone downward-transport event presented in the manuscript is also worthy of attention.

The overall research framework is reasonably complete. I am particularly interested in the relationship established in this study between lidar-observed ozone downward transport and variations in the temperature profile. The main conclusions of the current manuscript are generally reasonable. Nevertheless, the descriptions of several methods and the associated uncertainty analysis require further improvement. I recommend that the authors address the following comments in the revised manuscript.

Our Response:

We sincerely thank the reviewer for the positive assessment of the scientific significance of this study and the value of the simultaneous ozone and temperature lidar observations over the Tibetan Plateau.

Following the reviewer's suggestions, we have carefully revised the manuscript to improve the clarity and rigor of the analysis. In particular, we clarified the identification of the T0-T6 features and strengthened their event-by-event comparison with temperature variations. We also distinguished the direct lidar observations from their dynamical interpretation, clarified the respective roles of ERA5 and the lidar data, improved the discussion of tropopause folding and wave-related oscillations, and refined the cross-tropopause flux diagnosis. In addition, the descriptions of the lidar system, retrieval methodology, validation, and uncertainties have been expanded, and the identified errors have been corrected.

We believe that these revisions have substantially improved the manuscript. Detailed responses to the individual comments are provided below.

Comments and Suggestions #1

P. 4, Lines 95-99

The manuscript states that the raw backscatter signals were stored at 1 min intervals, while the stratospheric signals were accumulated over 30 min and processed using a moving window to obtain continuous profiles. Under this processing scheme, retrievals at adjacent output times may share a large proportion of the same raw signals. The authors should therefore distinguish between the effective integration time and the independent temporal resolution.

For example, the expression "1 min temporal resolution" could be revised to "a 1 min output interval with a 30 min effective integration time." These two concepts should not be treated as equivalent.

Our Response:

Thank you for the careful evaluation of our work and for your valuable suggestion. We have revised the corresponding description to clarify the temporal output interval and the presentation of the wavelength-dependent photon-count profiles and signal-to-noise ratios. We appreciate this comment, which has helped improve the clarity and methodological rigor of the manuscript.

Changes in the manuscript:

The corresponding description in Lines 144-148 of the revised manuscript has been revised as follows: "In routine operation, the system records raw signal files at a 1-min output interval … the resulting wavelength-dependent photon-count profiles and signal-to-noise ratios are shown in Fig. 2(a-d)."The corresponding revisions are highlighted in green in the revised manuscript.

Comments and Suggestions #2

P. 6, Lines 111-116

This section presents the merged ozone number-density profiles obtained from the lidar measurements, but no uncertainty range is provided. Considering that the ozone flux calculated later in the manuscript depends simultaneously on ozone concentration, mass flux, and the diagnosed tropopause position, the authors should provide a reasonable estimate of the uncertainty in the retrieved ozone profiles.

Our Response:

We thank you for the careful evaluation of our work and for the valuable suggestions.

The ozone lidar system employs six return wavelengths and ten signal channels, together with a range-dependent retrieval strategy using separate low and high-altitude channels, to ensure an adequate signal-to-noise ratio (SNR) over each altitude range. In the ozone retrieval, the altitude-dependent variation of the molecular absorption cross-sections associated with changes in atmospheric temperature is also taken into account. To construct a continuous ozone profile, the five retrieved profile segments are merged using three-bin overlap regions at the boundaries between adjacent segments. This multi-channel and range-dependent retrieval strategy helps reduce the retrieval uncertainty and ensures continuity between the different altitude ranges.

The detailed retrieval procedure, error analysis, and performance evaluation of the USTC Ozone Lidar have been reported in Fang et al. (2019), particularly in Figs. 7 and 8. In the revised manuscript, we have also expanded the relevant parts of Section 2 to provide a more accurate and rigorous description of the lidar configuration, retrieval procedure, profile merging, interference terms, validation, and principal sources of uncertainty.

Changes in the manuscript:

The descriptions of the lidar configuration, measurement channels, and data-acquisition strategy have been expanded in Lines 116-148. The retrieval procedure, profile merging, interference terms, validation, and principal sources of uncertainty are further clarified in Lines 153-165 of the revised manuscript.

Comments and Suggestions #3

P. 10, Lines 219-229

The authors select 3 PVU as the dynamical tropopause for this event based on changes in the calculated mass flux under different potential-vorticity thresholds and on the spatial continuity of the corresponding PV surfaces. This choice is generally understandable, but the current selection

criteria remain somewhat qualitative.
I suggest that the authors provide a comparison of the main results obtained using, for example, the 2, 3, and 4 PVU surfaces. If the principal conclusions remain consistent under these different thresholds, such a comparison would provide stronger evidence for the robustness of the results. Alternatively, the statement that "3 PVU is the most appropriate threshold" could be moderated. A more precise formulation would be that "3 PVU is adopted in this study as a representative threshold for this event."

Our Response:

Thank you for this helpful suggestion. The rationale for selecting 3 PVU as the dynamical-tropopause threshold is described in Lines 298-319 and illustrated in Figs. 6 and 7.
The sensitivity analysis in Fig. 6 shows that thresholds below 3 PVU produce relatively large upward and downward transport with stronger tropospheric characteristics, whereas thresholds above 3 PVU yield markedly smaller transport with stronger stratospheric characteristics. The zonal and meridional PV cross-sections in Fig. 7(a-b) further show that lower-PVU surfaces become discontinuous in some regions, while their continuity and stability improve for thresholds of 2 PVU and above. Based on both the flux sensitivity and the spatial structure of the PV surfaces, we adopt 3 PVU as a reasonable and representative dynamical-tropopause threshold for this event. The corresponding surface is indicated by the orange lines in Fig. 7(a-b).
Following the reviewer's suggestion, we have also replaced statements describing 3 PVU as "the most appropriate threshold" with the more precise wording "a representative dynamical-tropopause threshold for this event," including the corresponding statement in the Abstract (Lines 15-16).

Changes in the manuscript:

The rationale for selecting the 3-PVU dynamical tropopause has been clarified in Lines 298-319 of the revised manuscript. The revised text now describes both the sensitivity of the diagnosed upward and downward mass fluxes to different PV thresholds, as shown in Fig. 6, and the spatial continuity and stability of the corresponding PV surfaces, as shown in Fig. 7(a-b). The orange lines in Fig. 7(a-b) indicate the adopted 3-PVU dynamical tropopause.
In addition, statements describing 3 PVU as "the most appropriate threshold" have been moderated throughout the manuscript. They now state that "3 PVU is adopted as a reasonable and representative dynamical-tropopause threshold for this event." The corresponding wording in the Abstract has also been revised in Lines 15-16.

Comments and Suggestions #4

Pp. 8-13, Figs. 4 and 8 and the related discussion
The most distinctive aspect of this study is the simultaneous observation of high-resolution ozone and temperature profiles by the lidar system. I recommend that the authors further strengthen this part of the manuscript.
In particular, the identification criteria for the T0-T6 stages should be described more clearly. The manuscript should also explain more explicitly how the observed temperature gradients correspond to the ozone anomalies. A quantitative or event-by-event comparison would be especially useful. Further development of this analysis would make the observational contribution of the study more prominent. It would also reduce the extent to which the main conclusions depend on a single flux-diagnostic method.

Our Response:

We thank you for the careful evaluation of our work and for the valuable suggestions.
We agree that the co-located and co-temporal observations of ozone and temperature profiles constitute one of the most distinctive observational contributions of this study. Following the reviewer's recommendation, we have substantially expanded the discussion associated with Figs. 4 and 8 and have revised Sections 3.1 and 3.2 to make the identification and interpretation of the T0-T6 episodes more explicit.
First, we have clarified the observational criteria used to identify T0-T6. These labels denote coherent, short-lived episodes in which an ozone-enhanced structure near the tropopause can be tracked over adjacent moving-window retrievals and exhibits a discernible downward displacement relative to the surrounding observations. Only episodes for which co-temporal 387-nm Raman temperature profiles with an adequate signal-to-noise ratio were available over the corresponding altitude range were included in the comparison. We also clarify that T0-T6 are observational event labels used for comparative analysis and are not, by themselves, interpreted as direct proof of irreversible cross-tropopause transport.
Second, we have strengthened the event-by-event comparison between the ozone and temperature observations. For each episode, the temperature gradient is now evaluated over the same observation window and the corresponding altitude interval of the ozone-enhanced structure. The revised manuscript explicitly shows that six of the seven episodes (T0, T1, and T3-T6) are associated with temperature gradients exceeding 8 K km^{-1}, whereas T2 exhibits a weaker but still distinct gradient of 4.2 K km^{-1}.
We have also revised the discussion to distinguish more clearly between observational correspondence and dynamical interpretation. The co-temporal and co-altitudinal correspondence between the ozone displacements and temperature variations is presented as a direct lidar-based observational result, while the ERA5-derived PV fields and the Wei flux diagnostic are used subsequently to place these local observations within the regional dynamical context of the overall STE event. We no longer use the flux diagnostic as the sole basis for interpreting each individual T0-T6 feature.
These revisions strengthen the independent observational evidence provided by the simultaneous ozone and Raman-temperature measurements and reduce the extent to which the main interpretation depends on a single cross-tropopause flux-diagnostic framework. We thank the reviewer for this suggestion, which has helped us better highlight the principal observational contribution of the study.
Changes in the manuscript:
Sections 3.1 and 3.2 and the discussions associated with Figs. 4 and 8 have been revised. An event-by-event comparison of the ozone and temperature observations has also been added. The revised manuscript further distinguishes the direct observational correspondence between ozone and temperature variability from the subsequent dynamical interpretation. T0-T6 are now treated as observational event labels rather than direct evidence of irreversible cross-tropopause transport, while the ERA5-derived PV fields and Wei flux diagnostic are used to place these local observations within the regional dynamical context of the overall STE event.

Comments and Suggestions #5
P. 17, Lines 280-285
The description in this section is somewhat confusing. The authors are advised to carefully check the relevant text and clarify the intended meaning.

Our Response:

Thank you for pointing this out. We agree that the original description was confusing because it discussed the spatial pattern, domain-mean temporal evolution, and local contributions of the different mass-flux components within the same paragraph without clearly distinguishing among them.

We have carefully revised this section. In particular, we now clarify that the close similarity between the horizontal-advection term and the total flux in Fig. 9 refers primarily to the spatial distribution of the 6-h mean flux field. It does not imply that horizontal advection alone controls the net downward mass transport. In contrast, the domain-mean time series in Fig. 7(c-d) show that the horizontal- and vertical-motion contributions are largely compensating, such that variations in the tropopause-motion term exert an important influence on the temporal evolution of the net flux. At the Yangbajing lidar site, the vertical-motion term also contributes locally to the diagnosed downward flux.

We have therefore revised the paragraph to distinguish clearly between (1) the component controlling the regional spatial heterogeneity of the flux, (2) the component influencing the domain-mean temporal evolution, and (3) the local contribution at the lidar site.

Changes in the manuscript:

The corresponding revisions can be found in Lines 378-385 of the revised manuscript.

Comments and Suggestions #6

P. 17, around Line 343

The reference “shown in Fig. 10” appears to refer to Fig. 11. Please check and correct the figure citation.

Our Response and changes in the manuscript:

Thank you for your careful review and for raising this point. We have revised the manuscript accordingly; please see Lines 454-455 of the revised manuscript.

Response to Referee 3

We would like to thank the reviewer for the efforts and time and appreciate the encouraging review. Thank you for pointing out our mistakes. We really believe that your feedback has helped us to improve the presentation of our manuscript and the quality of our paper.

General Remarks

Because of unique terrain and atmospheric circulation, the Tibetan Plateau is a hotspot for studying troposphere-stratosphere exchange. Observation data from spaceborne sensors and reanalysis data were employed in the studying of troposphere-stratosphere exchange over the Tibetan Plateau, however, observation data with high spatial and temporal resolutions are still very lack, which are essential for studying troposphere-stratosphere exchange.

This article presents ozone measurements from a mobile ozone lidar located in the Tibetan Plateau, and study the troposphere-stratosphere exchange by using ozone as a tracer. Due to the high altitude, there are few lidar operated in the Tibetan Plateau. The lidar employed in the article has a capability of profiling ozone and temperature in the troposphere and stratosphere synchronously with high spatial and temporal resolutions, and the lidar data are very valuable for the atmospheric studying over the Tibetan Plateau. The job in the article is a good attempt to study the troposphere-stratosphere exchange by using ozone lidar data in the Tibetan Plateau. The consistency of the lidar measurements and ERA5 data indicated the reasonable of the EAR5 data over the Tibetan Plateau, and more details could be found in the lidar data, and these details could provide more information of the troposphere-stratosphere exchange.

The article could be accepted and published.

Our Response:

We sincerely thank the reviewer for the positive assessment of our manuscript and for recognizing the scientific value of the simultaneous high-resolution ozone and temperature lidar observations over the Tibetan Plateau. We also appreciate the reviewer's recognition that the lidar data provide fine-scale information complementary to satellite and ERA5 datasets. Following the reviewer's comments, we have carefully revised the manuscript to improve its methodological description, physical interpretation, uncertainty discussion, and overall clarity. We are grateful for the constructive suggestions and recommendation for publication.

Comments and Suggestions #1

1. Line 126, "USTC Ozone lidar shows good consistency the ERA5", however, in the figure 3(b), the peak value of the ozone concentration profile from ERA5 is obviously lager than the peak value from lidar.

Our Response:

Thank you very much for your helpful comment and suggestion. Our interpretation is as follows. ERA5 is a gridded reanalysis product that represents an analyzed atmospheric state over a finite horizontal grid cell, model level, and temporal sampling interval. Therefore, even after the ERA5 data are interpolated to the lidar site and to an altitude of 25 km, the ERA5 and lidar results do not represent strictly identical quantities because of their different spatial, vertical, and temporal representativeness.

Another possible explanation is that the ozone retrievals over approximately 20-32 km are based on the N_2 Raman backscatter signals. The reduced effective vertical resolution at these altitudes, together with the smoothing applied during the retrieval, may attenuate sharp ozone maxima and produce a smoothing-induced reduction in peak amplitude. Nevertheless, the main focus of the present study is the tropopause region between approximately 14 and 17 km, where the retrieved ozone profiles show no apparent abnormal behavior.

Changes in the manuscript:

We have revised the corresponding description in Lines 181-183 of the manuscript as follows: "Overall, the ozone profiles retrieved from the USTC Ozone Lidar exhibit … robust and complementary constraints." The corresponding revisions are highlighted in blue in the revised manuscript.

Comments and Suggestions #2

2. Line 171, the vertical resolution of the temperature profile from ERA5 for tropopause determination should be given.

Our Response:

Thank you very much for your helpful comment and suggestion. For the PV-based dynamical-tropopause diagnosis, the ERA5 fields were treated in pressure coordinates and vertically interpolated at uniform intervals of 0.5 hPa. For the initial ERA5-based screening of the event, however, the thermodynamic tropopause was identified using the height and temperature information corresponding to each interpolated pressure level, following the WMO lapse-rate criterion.

Changes in the manuscript:

We have clarified this procedure in Lines 238-239 of the revised manuscript as follows:
"For the initial ERA5-based screening of the event, the ERA5 fields were vertically interpolated at uniform 0.5-hPa intervals, and the thermodynamic tropopause was then identified from the corresponding height and temperature profiles according to the WMO lapse-rate criterion."
The corresponding revision is highlighted in blue in the revised manuscript.

Comments and Suggestions #3

3. The time in the article is the local time or UTC?

Our Response and changes in the manuscript:

Thank you for this question. All times reported in the manuscript are given in Coordinated Universal Time (UTC), rather than local time. We have clarified this time convention in the revised manuscript.

After the modification, we found the reviewer's comments are quite helpful. Once again, we appreciate for your warm work earnestly, and hope that the correction will meet your standards.

Best Regards.
Yours Sincerely,
All authors

Ozone Downward Flux Revealed by High-Resolution Differential Absorption Lidar over Tibet during Stratosphere-Troposphere Exchange

Ruichun Dong[1], Xin Fang[1,2], Chengyun Yang[1,2], Tao Li[1,2]

[1]National Key Laboratory of Deep Space Exploration/School of Earth and Space Sciences, University of Science and Technology of China, Hefei, Anhui, China

[2]CAS Center for Excellence in Comparative Planetology/CAS Key Laboratory of Geospace Environment/Mengcheng National Geophysical Observatory, University of Science and Technology of China, Hefei, Anhui, China

Correspondence to: Xin Fang (xinf@ustc.edu.cn)

Abstract. This study characterizes a prominent ozone intrusion event driven by stratosphere-to-troposphere exchange that occurred on 18-19 October 2017. The analysis is enabled by high spatiotemporal resolution ozone profile observations from the USTC Ozone Lidar deployed at Yangbajing, Tibet (29°N, 99°E). The high-spatiotemporal-resolution lidar observations resolve a series of short-lived, rapid ozone descent episodes during the STE event. Temperature profiles independently retrieved from the simultaneously measured 387-nm N_2 Raman signal further reveal a close temporal correspondence between these ozone descent episodes and temperature variations in the tropopause region, with temperature gradients exceeding 8 K km^{-1} for six of the seven identified episodes. Based on Wei's flux diagnostic and a sensitivity test of PV-based dynamical tropopause thresholds, 3 PVU is adopted as the representative threshold for this event. ECMWF Reanalysis v5 (ERA5) is then used to characterize the spatiotemporal evolution of cross-tropopause mass fluxes over 25-28°N, 95-99°E, showing that the ozone variations observed by the lidar were modulated by gravity waves associated with the tropopause fold. In addition, lidar-measured ozone profiles are incorporated into a cross-tropopause ozone flux calculation framework, yielding an instantaneous peak STE ozone flux of about 3-4·10^{-10}·kg·s^{-1}·m^{-2}, slightly higher than the corresponding ERA5 value, while maintaining strong agreement in overall flux magnitude and temporal evolution throughout the event. These results show that high-resolution vertical ozone observations and Raman-retrieved temperature profiles from the USTC Ozone Lidar, combined with wind field data, enable accurate quantification of STE-related ozone fluxes. This approach facilitates in-depth investigation of coupled atmospheric composition and dynamical processes.

1 Introduction

Stratosphere-Troposphere Exchange (STE) has been investigated for several decades and is recognized as a key process controlling the budgets of ozone, water vapor, and other trace constituents in the upper troposphere and lower stratosphere (UTLS) (Chen et al., 2006; Stohl et al., 2003). STE exerts a strong influence on upper-tropospheric ozone and plays an important role in the UTLS radiative budget, dynamical structure, chemical processing, and microphysical evolution (Lelieveld and Dentener, 2000). At the global scale, STE is associated with the large-scale atmospheric circulation, while individual exchange events occur over a wide range of spatial and temporal scales and are strongly modulated by synoptic-scale and mesoscale dynamical processes (Holton et al., 1995; Stohl et al., 2003). In the extratropics, tropopause folds, cutoff lows, upper-level jets, and wave-related disturbances have been identified as key mechanisms facilitating the transport of stratospheric air into the troposphere (Stohl et al., 2003). In particular, tropopause folds are closely related to upper-level frontogenesis and jet-stream dynamics and constitute an important pathway for cross-tropopause exchange. The subtropical jet is particularly relevant in this context because its strong horizontal and vertical wind shear favors tropopause deformation and folding. Global analyses by Sprenger et al. (2003) showed pronounced stratosphere-to-troposphere transport (STT) in the subtropical region and demonstrated that tropopause folds occur preferentially in the subtropics, with a substantial fraction of cross-tropopause exchange events between 20° and 40° latitude being associated with such folds. Subsequent global climatological analyses further demonstrated pronounced geographical and seasonal variations in tropopause-fold occurrence and its relationship with cross-tropopause transport (Škerlak et al., 2015).

Ozone is a particularly effective tracer for investigating stratosphere-to-troposphere transport due to the strong contrast in ozone abundance between the stratosphere and troposphere. Accordingly, cross-tropopause ozone transport has been extensively studied using numerical models, satellite observations, ozonesondes, aircraft measurements, and ground-based remote sensing. For example, Olsen et al. (2004) quantified the relationship between extratropical cross-tropopause mass flux and ozone flux, demonstrating that ozone transport depends on both mass exchange and ozone concentration near the tropopause.

Internationally, a variety of observational and modeling studies have further advanced the understanding of STE structure and its fine-scale variability. High-resolution ground-based ozone lidar measurements are particularly valuable for resolving thin and rapidly evolving ozone-rich layers associated with stratospheric intrusions. Eisele et al. (1999) demonstrated that high-vertical-resolution lidar observations can capture fine structures associated with tropopause folds and stratospheric intrusion events. In addition, Kuang et al. (2012) combined ground-based ozone lidar and ozonesonde observations with meteorological and potential vorticity analyses to characterize a stratospheric intrusion associated with a cutoff cyclone and tropopause fold, highlighting the capability of integrated observational systems to diagnose STE processes. These studies collectively demonstrate that high-resolution ozone profiling is essential for resolving the fine-scale structure and temporal evolution of STE events, which are often poorly represented in satellite observations and coarse-resolution reanalysis datasets.

Despite these advances, the spatial and temporal characteristics of STE exhibit pronounced regional variability. The Tibetan Plateau lies within the subtropical latitude band and is strongly influenced by the upper-level subtropical jet, making jet-related tropopause deformation and folding particularly relevant to cross-tropopause transport over this region. Shaped by its distinctive topography and circulation systems, the Tibetan Plateau and its surrounding regions display unique patterns of atmospheric composition and dynamical structure, imparting strong regional characteristics to STE. As a result, this high-elevation domain serves as a key corridor and observational window for energy and mass exchange between the stratosphere and troposphere, with important implications for understanding coupled atmospheric processes on the global scale (Yang et al., 2004; Chen et al., 2010).

Given that STE is a major physical mechanism governing the distribution and variability of atmospheric trace constituents in the UTLS, extensive observational and modeling studies have been conducted over the Tibetan Plateau, with particular attention to ozone and the mechanisms shaping its distribution. For example, Zhou and Zhang (2005) used TOMS satellite data to identify a summertime minimum in total-column ozone over the Plateau, commonly referred to as the Tibetan ozone valley, and related it to atmospheric ascent over the elevated terrain. Subsequent studies further demonstrated that both thermodynamic and dynamical processes contribute to the formation and maintenance of this summertime ozone minimum (Randel and Park, 2006; Randel et al., 2010). Using TOMS observations and model simulations, Tian et al. (2008) showed that the elevated summertime tropopause over the Tibetan Plateau modifies the vertical distribution of ozone in the UTLS. In addition, based on ozonesonde observations over the northeastern Tibetan Plateau, Chen et al. (2012) identified signatures of stratospheric air intruding into the troposphere along the periphery of the upper-tropospheric anticyclone. These studies collectively demonstrate that the distinctive topography and circulation of the Tibetan Plateau exert strong influences on regional ozone distributions and STE processes.

Using a springtime tropopause-folding event over the northeastern Tibetan Plateau, Zhang et al. (2010) showed that an upper-level jet associated with an intruding low-pressure trough played an important role in driving cross-tropopause exchange, with both TST and STT occurring during the event evolution. Nevertheless, compared with other regions where long-term ozonesonde, aircraft, and ground-based remote sensing observations are available, high-spatiotemporal-resolution observations of STE over the Tibetan Plateau remain limited. This limitation makes it difficult to resolve short-lived and vertically confined ozone structures and to quantify their relationship with rapid dynamical and thermal variability near the tropopause.

To address this observational gap, we developed a mobile differential absorption lidar (DIAL) system (Fang et al., 2019) capable of high-spatiotemporal-resolution, long-duration profiling of ozone in both the troposphere and stratosphere. Based on measurements from this platform, we present a comprehensive analysis of an STE-related ozone descent event over Tibet. Section 2 describes the datasets used in this study, with emphasis on the mobile differential absorption ozone lidar deployed at Yangbajing, Tibet, and presents intercomparisons and accuracy validation of the retrieved ozone profiles. In Section 3, we corroborate the STE-related ozone descent detected by the lidar using ERA5 reanalysis fields; we then select an appropriate tropopause definition and diagnose cross-tropopause mass fluxes over the observational domain, quantifying the spatial distribution of the mass flux across the tropopause. Building on these diagnostics, we combine the lidar-measured ozone profiles with ERA5 wind fields to estimate cross-tropopause ozone fluxes, enabling a quantitative, observation-based assessment. Section 4 summarizes the main conclusions and outlines directions for future work.

2 Data sources and lidar system overview

The data used in this study were acquired with a mobile differential absorption lidar (USTC Ozone Lidar) system deployed by our group at Yangbajing, Tibet (29°N, 99°E), which enables simultaneous observations of ozone in both the troposphere and stratosphere. The complete system configuration, technical specifications and performance characterization have been described in detail by Fang et al. (2019). Here, we summarize only the key instrumental parameters directly relevant to the observations and analyses presented in this study. Satellite imagery of the lidar site in Tibet and the on-site layout of the ozone lidar system are shown in Fig. 1(a-b), respectively. After performance tuning and testing in Huainan, Anhui Province, the mobile ozone lidar system was transferred to Yangbajing for routine observations beginning in October 2017. It is one of the few mobile DIAL stations worldwide capable of simultaneously profiling tropospheric and stratospheric ozone (McDermid et al., 1991; Godin-Beekmann et al., 2003; Hansen et al., 2003; Baray et al., 2013), and represents a distinctive example of such a system operating at the highest altitude among comparable platforms globally (approximately 4300 m above sea level). Ground-based ozone lidar has also been extensively applied to studies of STT and stratospheric intrusions. Previous studies have demonstrated the capability of ozone lidar to resolve ozone-rich layers associated with cross-tropopause exchange and tropopause-folding events (Ancellet et al., 1991; Eisele et al., 1999). Subsequent lidar observations have been used to investigate the descent, evolution, and mixing of stratospheric ozone intrusions in the free troposphere (Langford et al., 2009; Kuang et al., 2012). More recently, long-term ozone lidar observations have further demonstrated the frequent occurrence and substantial influence of stratospheric intrusion layers in the free troposphere (Trickl et al., 2020). These studies demonstrate the important role of high-resolution ozone lidar observations in characterizing the fine-scale structure and temporal evolution of STT.

The mobile differential absorption ozone lidar combines the differential absorption technique with distinct backscattering mechanisms. Schematics of the mobile ozone DIAL system and of the emission reception configuration for the different detection wavelengths are shown in Fig. 1(c) and 1(d), respectively. Multiple wavelengths are employed to accommodate the large difference in ozone abundance between the troposphere and stratosphere and the corresponding requirements for differential-absorption sensitivity and detection range. For tropospheric ozone measurements, where ozone abundance is relatively low, the system employs the 289/299-nm DIAL pair to provide sufficient differential ozone absorption sensitivity. These two wavelengths are generated through stimulated Raman scattering by separately pumping D_2 and H_2 Raman cells with 266-nm radiation obtained from the fourth harmonic of a Nd:YAG laser, producing the first-order Stokes wavelengths near 289 and 299 nm, respectively (Papayannis et al., 1999; Kourtidis et al., 2002; Fang et al., 2019).For stratospheric ozone measurements, where ozone abundance is substantially higher, the system employs the 308/355-nm DIAL pair. The ozone-absorbing wavelength at 308 nm is directly generated by a XeCl excimer laser, whereas the reference wavelength at 355 nm is generated through third-harmonic generation of the 1064-nm fundamental output of a Nd:YAG laser. This 308/355-nm configuration has been widely employed in stratospheric ozone DIAL systems (McDermid et al., 1991; Godin-Beekmann et al., 2003; Fang et al., 2019). In addition to the elastic backscatter signals at the transmitted wavelengths, N_2 vibrational Raman returns at 332 and 387 nm, corresponding to excitation at 308 and 355 nm, respectively, are simultaneously detected (McGee et al., 1993). These Raman channels provide additional information for reducing aerosol/backscatter-related effects on the ozone retrieval. In the receiver subsystem, four independent telescopes, each with a 1.25 m aperture, are combined into a collecting array with an effective diameter exceeding 2.2 m to detect signals at 308, 332, 355, and 387 nm, enabling ozone measurements from the tropopause to the upper stratosphere over an altitude range of 18-50 km. This array-based design enhances the signal-to-noise ratio for stratospheric observations. A separate 1 m aperture prime-focus telescope receives the 289 and 299 nm signals for ozone detection over 8-19 km above sea level, while two 0.21 m aperture Newtonian telescopes receive the same wavelengths for measurements over 5-10 km above sea level, thereby extending coverage from the troposphere to the lower stratosphere across 5-19 km above sea level. Together, the seven telescopes provide simultaneous ozone profiling from 5 to 50 km above sea level, spanning both the troposphere and stratosphere.

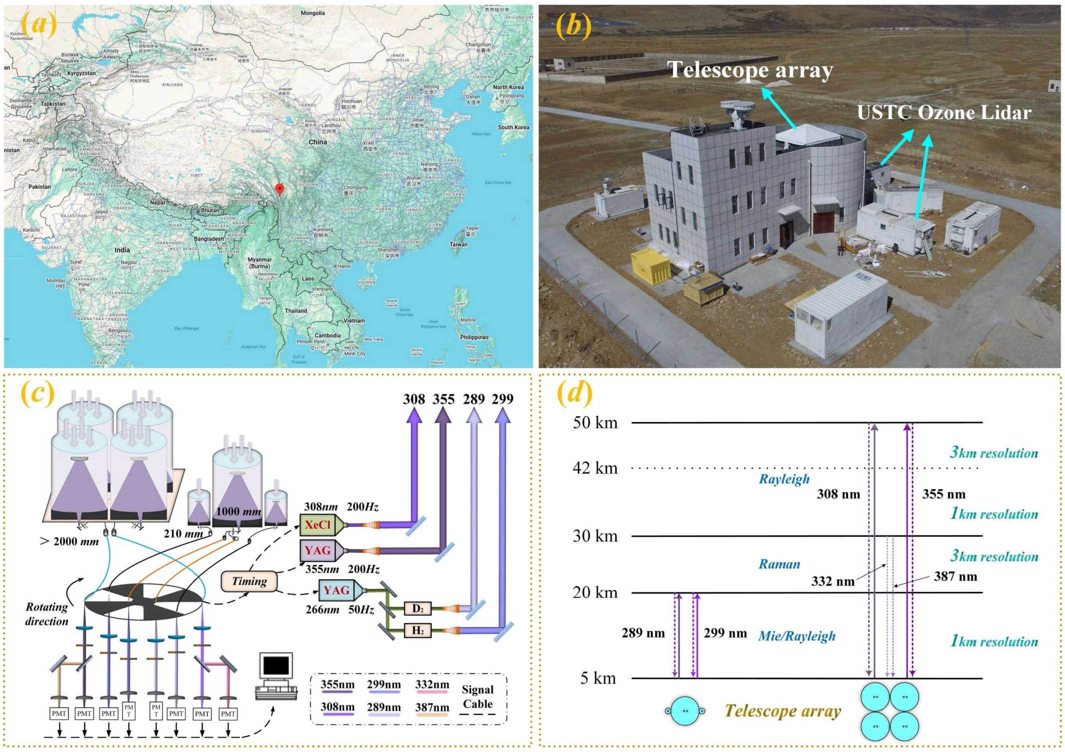

Figure 1: (a) Satellite image of the radar observation site on the Tibetan Plateau (Map data © Google Earth 2026); (b) Field layout of the ozone lidar system; (c) Schematic of the mobile ozone lidar system; (d) Altitude ranges corresponding to different laser emission wavelengths.

To ensure accurate ozone measurements, the laser beam axis must be properly aligned with the receiving telescope, and the telescope field of view must adequately overlap with the laser emission field. As shown in Fig. 1(c), a mechanical chopper was placed in the optical path to reduce noise from strong near-field backscatter. In routine operation, the system records raw signal files at a 1-min output interval, with a vertical bin size of 61.44 m and 2,048 range bins. For stratospheric ozone retrieval, the 1-min photon-counting signals are accumulated to achieve an effective integration time of 30 min, thereby ensuring sufficient signal quality in the stratosphere. After saturation correction, the resulting wavelength-dependent photon-count profiles and signal-to-noise ratios are shown in Fig. 2(a-d). As shown in Fig. 2, the SNR is sufficient across the altitude ranges corresponding to the different wavelengths presented in Fig. 1(c-d).

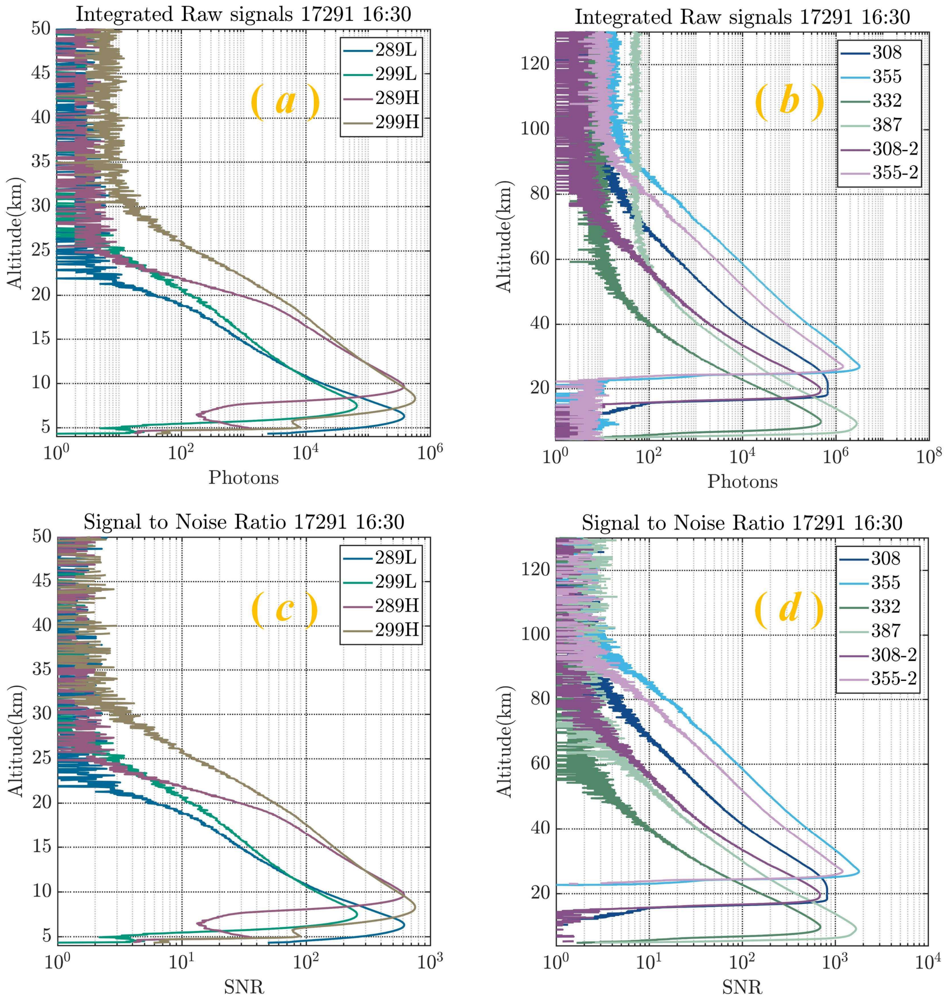

Figure 2: Wavelength-dependent photon returns and corresponding signal-to-noise ratios for the mobile ozone DIAL system (USTC Ozone Lidar).

Background noise, averaged over the altitude range of 115-125 km, was subtracted from the raw signals. After denoising the raw backscattered optical signals using wavelet-transform-based signal processing (Fang and Huang, 2004; Yin and Wang, 2006; Boggess and Narcowich, 2009), ozone number-density profiles were retrieved using the differential absorption lidar (DIAL) equation (Kovalev and Eichinger, 2004). The retrieval considers several important factors affecting the retrieved ozone number density, including the temperature dependence of the ozone absorption cross-sections, absorption by interfering atmospheric species, and wavelength-dependent molecular and aerosol backscatter and extinction (Gimmestad, 2005).

Aerosols and clouds represent additional sources of uncertainty in ozone DIAL measurements. Differences in aerosol backscatter and extinction between the online and offline wavelengths can introduce systematic errors, particularly in the presence of strong vertical gradients in aerosol loading (Browell et al., 1985; Kovalev and Bristow, 1996). Additional wavelength and Raman measurements can help constrain these aerosol-related contributions. In the USTC Ozone Lidar, the N_2 vibrational Raman returns at 332 and 387 nm provide complementary information for reducing aerosol/backscatter-related effects in the upper-tropospheric and stratospheric ozone retrievals. The retrieved ozone profiles are further evaluated in the present study through comparisons with ERA5 and independent Aura satellite observations, as shown in Fig. 3.

The ozone number density profiles retrieved from the lidar observations over five altitude intervals are shown in Fig. 3(a). Because differences in detection wavelength, laser pulse energy, and telescope field of view determine the effective retrieval range for each channel, the five profile segments were merged using 3-bin overlap regions to produce a continuous ozone profile. The merged profile was then compared with ERA5 data at the corresponding time, and further cross-validated against observations from the Ozone Monitoring Instrument (OMI; Liu et al., 2010) and the Microwave Limb Sounder (MLS; Waters et al., 2006) aboard the Aura satellite (Schoeberl et al., 2006), as shown in Fig. 3(b).

The results show that the ozone profile retrieved from USTC Ozone Lidar agrees well overall with ERA5. It should be noted, however, that satellite observations are constrained by orbital sampling and overpass timing. On this day, the MLS overpass occurred at 18:50 UT at 25.22°N, 105.20°E. Below 25 km, the observed ozone concentrations were broadly consistent with the USTC Ozone Lidar measurements, whereas above 25 km, MLS showed systematically higher ozone concentrations at the same altitudes. This discrepancy is likely related to the large spatial separation between the satellite overpass location and the lidar site. By contrast, the OMI overpass occurred at 07:10 UT at 27.07°N, 99.34°E. Above 25 km, the ozone concentrations agreed well with the USTC Ozone Lidar retrievals, whereas below 25 km, OMI exhibited a certain positive bias relative to the lidar measurements. Although the spatial distance between the satellite footprint and the lidar station was minimized, the relatively long temporal separation between the OMI overpass and the lidar observations at the same location may still have introduced appreciable differences in ozone concentration. Overall, the ozone profiles retrieved from the USTC Ozone Lidar exhibit good consistency in their overall trends with ERA5, with the two datasets providing robust and complementary constraints. Moreover, the high spatiotemporal sampling capability of the lidar allows it to resolve vertically confined and short-lived ozone structures that are often missed by other datasets, since satellite profile data typically contain only about a dozen vertical points and ERA5 records only slightly more than 30 pressure levels. In particular, the lidar observations resolve short-lived ozone descent structures occurring on sub-hourly (approximately 30 min) to 1-2 h, as discussed in Section 3.1. This capability is particularly valuable for detecting and analyzing transient cross-tropopause ozone transport events.

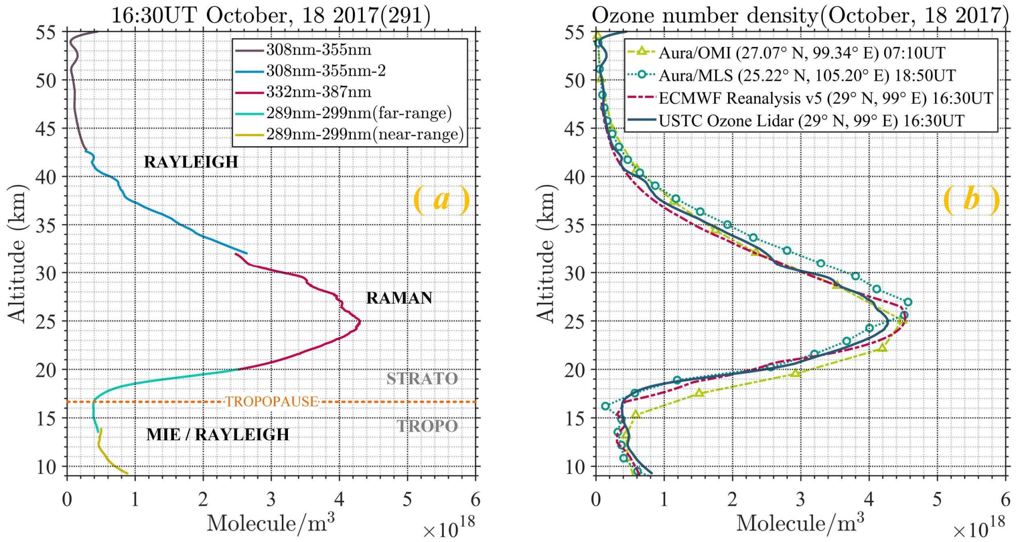

Figure 3: (a) Retrieved ozone concentration profiles from the ozone lidar over different altitude ranges; (b) Comparison of the merged ozone profile with ERA5 reanalysis and Aura/OMI and Aura/MLS satellite observations. The labels "MIE/RAYLEIGH," "RAYLEIGH," and "RAMAN" in panel (a) indicate the different backscatter signals used for ozone retrieval: MIE/RAYLEIGH denotes the elastic Mie and Rayleigh backscatter signals at 289 and 299 nm used for tropospheric ozone retrievals; RAYLEIGH denotes the elastic Rayleigh backscatter signals at 308 and 355 nm used for stratospheric ozone retrievals; and RAMAN denotes the N_2 vibrational Raman backscatter signals at 332 and 387 nm, corresponding to excitation at 308 and 355 nm, respectively.

3 Methods and Results

3.1 Lidar observations and supporting evidence for a STE-related ozone descent event

The USTC Ozone Lidar deployed at Yangbajing, Tibet (29°N, 99°E) was developed in-house by the University of Science and Technology of China. The system enables simultaneous profiling of ozone in the troposphere and stratosphere with high spatial and temporal resolution, providing a particularly valuable observational constraint on ozone variability over the Tibetan Plateau, where in situ data remain sparse. The lidar retrievals also allow us to identify clear signatures of downward ozone transport. Influenced by its unique high elevation topography and the Asian monsoon, the Tibetan Plateau is recognized as one of the most active regions for Stratosphere-Troposphere Exchange (STE) (Chen et al., 2006). Under these conditions, ozone transport from the stratosphere across the tropopause is likely to be an important source of background tropospheric ozone over Tibet, with potential implications for regional climate regulation and for the global coupling of chemistry and climate (Gettelman et al., 2002; Duan et al., 2005). In this section, we use ERA5 global reanalysis fields (0.25° × 0.25° spatial resolution; 1 h temporal resolution) as supporting evidence to analyze the STE event captured by the ozone-profiling lidar and to provide an initial observational assessment of its evolution.

As shown in Fig. 4, the USTC Ozone Lidar captures pronounced temporal variations in the vertical distribution of ozone near the tropopause during the nights of 18 and 19 October 2017. To ensure an adequate signal-to-noise ratio, photon-counting returns were accumulated over 30 mins and processed using a moving time-window method (Duchnowski et al., 2025), yielding a continuous ozone concentration distribution as a function of altitude and time. It is worth noting that ozone DIAL measurements are conducted only at night and are limited by weather conditions. As a result, the ozone results typically appear as banded segments separated by temporal gaps, shown in Fig. 4. Figure 4(a) shows the evolution observed during 16:00-21:00 on 18 October. An ozone-enhanced layer exhibits a pronounced downward displacement in the time-altitude cross-section, forming the tilted structure indicated by the blue arrow. Figure 4(b) shows the subsequent evolution during 15:00-21:00 on 19 October, when the ozone-enhanced structure exhibits an overall upward displacement, as indicated by the orange arrow. At this stage of the analysis, these features are interpreted descriptively as vertical displacements of ozone-rich structures near the tropopause; whether they represent irreversible cross-tropopause transport or primarily reflect tropopause displacement is examined using the dynamical and flux diagnostics presented below.

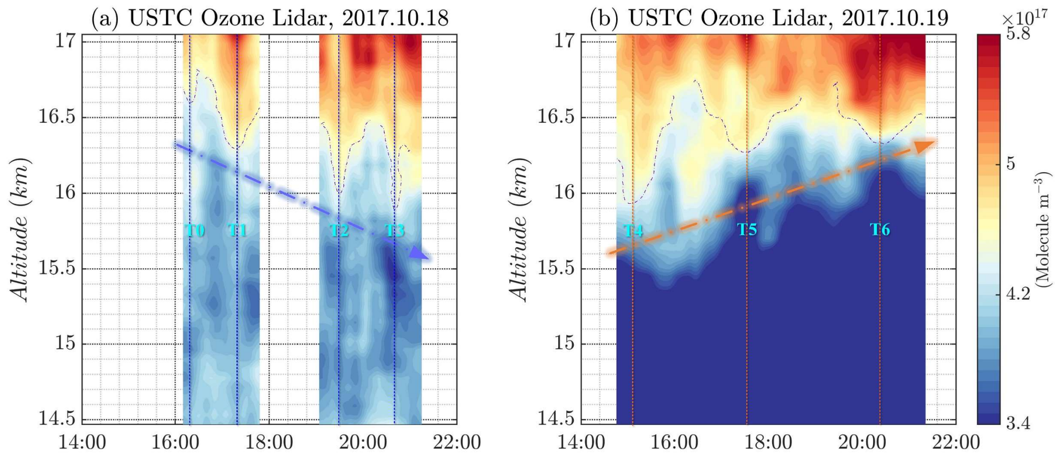

Figure 4: Temporal evolution of the ozone distribution near the tropopause observed by the USTC Ozone Lidar on (a) 18 October and (b) 19 October 2017. The blue arrow in (a) indicates the downward displacement of the ozone-enhanced structure, whereas the orange arrow in (b) indicates its overall upward displacement during the subsequent evolution. T0–T6 mark the short-lived downward-displacement episodes discussed in the text.

Within these broader variations, the lidar resolves several short-lived episodes of downward displacement of ozone-enhanced structures, marked T0-T6 in Fig. 4. Some episodes persist for 1-2 h, whereas others last for less than 1 h. Their short duration highlights the capability of the lidar to resolve rapid variability in ozone structure near the tropopause that may not be captured by satellite observations or lower-resolution meteorological datasets. Previous studies have given comparatively limited attention to such short-lived ozone structures near the tropopause. Importantly, these features should not necessarily be interpreted as individual cross-tropopause transport events, since rapid tropopause oscillations or undulations may also produce apparent vertical displacements of ozone-rich layers. Their repeated occurrence on sub-hourly to hourly timescales nevertheless provides a useful observational perspective on fine-scale ozone variability and tropopause dynamics. The relationship of these features to tropopause variability and cross-tropopause transport is examined further using the temperature, dynamical, and flux diagnostics presented below.

To corroborate the suspected STE-related ozone descent observed by the ozone lidar in autumn 2017, we further use ERA5 global reanalysis fields as an independent line of evidence. A prerequisite for diagnosing cross-tropopause exchange during STE events is a robust identification of the tropopause. For an initial ERA5-based screening of the event (interpolate the ERA5 data at uniform intervals of 0.5 hPa), the tropopause altitude is determined using the thermodynamic definition. Following the World Meteorological Organization (WMO) lapse-rate criterion proposed in 1986 (Wei et al., 1987), the thermodynamic tropopause is defined as the lowest level above the 500 hPa surface at which the atmospheric temperature lapse rate decreases to 2 °C km^{-1} or less, provided that the mean lapse rate within the 2 km layer above this level does not exceed 2 °C km^{-1}. In this study, the thermodynamic tropopause was determined independently at each available ERA5 time step (1 hour). Specifically, the temperature lapse rate was calculated from the corresponding ERA5 vertical temperature profile, and the WMO lapse-rate criterion was then applied to identify the tropopause. Thus, both the temperature lapse rate and the resulting tropopause altitude were allowed to vary with time. Analysis of ERA5 data during the periods covered by USTC Ozone Lidar observations reveals a pronounced cross-tropopause ozone descent event. We therefore focus on ERA5 data at the Yangbajing site for 16-19 October 2017. The continuous temporal coverage provided by ERA5 during this period allows the evolution of the event to be captured more completely, as illustrated in Fig. 5(a). A strong STE-related ozone descent is evident during 18-19 October 2017, in close agreement with the USTC Ozone Lidar observations.

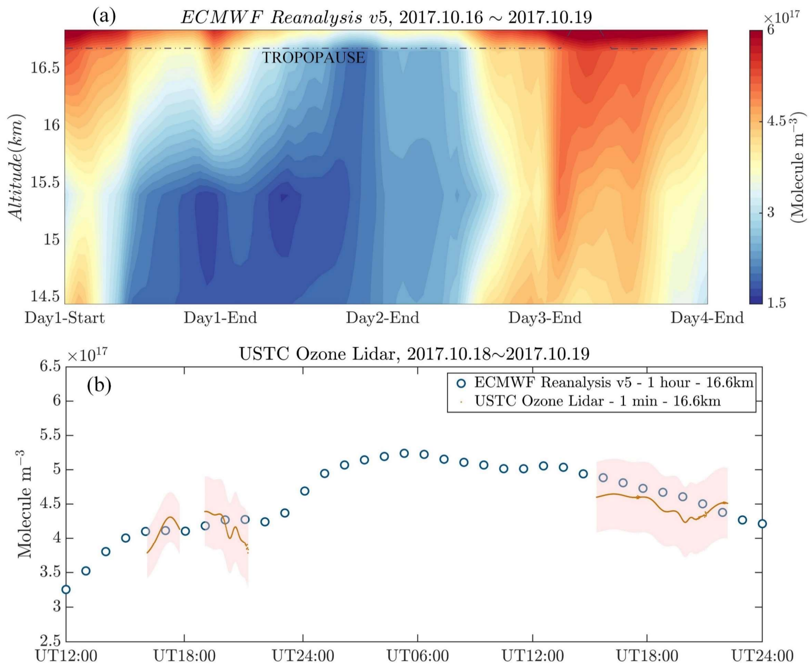

Figure 5: (a) ERA5 depiction of the STE evolution near the tropopause over Yangbajing during 16–19 October 2017; (b) Comparison of lidar-observed and ERA5 ozone concentrations at the tropopause level (16.6 km) during 18-19 October 2017.

Both the USTC Ozone Lidar observations and ERA5 capture the onset and recovery phases of this ozone descent event. Differences between the lidar-retrieved ozone concentrations and those from ERA5 are further quantified. As shown in Fig. 5(b), the ozone number density variations observed by the USTC Ozone Lidar during the STE event are compared with the corresponding ERA5 values. To ensure a consistent comparison, the analysis is performed at the tropopause level (16.6 km), and the 95% confidence interval of the lidar retrievals is also shown. Notably, ERA5 provides hourly-resolution data, whereas the ozone lidar yields full-profile ozone measurements with 1-min update intervals. Figure 5(b) shows that the tropopause-level (16.6 km) ozone number densities measured by the USTC Ozone Lidar during 18-19 October 2017 agree closely with ERA5 in both absolute magnitude and temporal evolution. However, comparing Fig. 5(a) with Fig. 4(b) indicates that during the recovery phase on 19 October 2017, the ozone number densities retrieved by USTC Ozone Lidar below 15.5 km are systematically slightly lower than those in ERA5. Given the high SNR of the lidar returns during this period, the discrepancy is more likely to reflect a modest overestimation by ERA5 of the ozone number density associated with stratosphere-to-troposphere transport at this stage.

3.2 Tropopause definition and cross-tropopause flux diagnostics

Mass and trace-constituent exchange between the stratosphere and troposphere is a central component of the coupled troposphere–stratosphere system. In 1987, Wei proposed a diagnostic framework for quantifying this exchange, in which all physical processes contributing to cross-tropopause transport can be expressed in an explicit mathematical form (Reiter., 1975; Wirth et al., 1999). The general form can be written as:

$$F(f) = [\rho J_\eta f \left(\frac{d\eta}{dt} - \frac{\partial\eta}{\partial t_{z_0}} - \vec{U}\cdot\nabla_{z_0}\eta\right)]_{\eta_B}, \quad (1)$$

where $F(f)$ is the air mass flux across the tropopause, ρ is the air density near the tropopause, η is a generalized vertical coordinate, $J_\eta = \partial z/\partial\eta$ is the vertical coordinate-transformation factor between the generalized vertical coordinate η and geometric altitude z, z_0 denotes the tropopause, $d\eta/dt$ is the vertical velocity in η coordinates, $\vec{U}$ is the horizontal wind vector, and f is the constituent mixing ratio. In pressure coordinates, this expression becomes:

$$F(\rho) = -g^{-1}\left(w - \vec{U}\cdot\nabla_{z_0}p - \frac{\partial p}{\partial t_{z_0}}\right), \quad (2)$$

A key advantage of Wei's diagnostic formulation is that it allows the upward and downward cross-boundary fluxes to be computed separately and can be applied to any atmospheric constituent across an arbitrary reference surface. Given the large contrast in ozone mass mixing ratios between the stratosphere and troposphere, and the common assumption that an air mass becomes well mixed over a relatively short timescale after crossing the tropopause, quantitative assessments based on ozone profiles require the upward and downward fluxes to be treated separately. As noted above, we initially located the thermodynamic tropopause using changes in the vertical temperature lapse rate. In some situations, however, particularly near jet streams, this tropopause can be poorly defined. Because the following analysis examines lidar observations in detail and because the Yangbajing site lies in the low-to-mid latitudes, where large-scale dynamics and strong disturbances can substantially perturb the thermal structure, defining the tropopause solely from lapse-rate criteria may introduce appreciable uncertainty.

Holton noted that the tropopause is better regarded as a quasi-material surface (Holton et al., 1995). This perspective is well captured by the dynamical tropopause defined in terms of potential vorticity (PV), and cross-tropopause transport studies therefore commonly adopt a PV-based tropopause, typically using thresholds in the range of 1.5-4 PVU (where PVU denotes the potential vorticity unit). Moreover, Yang et al showed that the choice of PV threshold can substantially affect estimates of cross-tropopause exchange, and advocated selecting an optimal threshold based on its correlation with observations or diagnostic quantities (Yang et al., 2003). It should be noted that the PV fields used here are derived from ERA5 and therefore cannot be expected to reproduce the fine-scale structures resolved by the lidar on a point-by-point or event-by-event basis. In this study, the ERA5-derived PV is used primarily to characterize the regional dynamical tropopause and the larger-scale dynamical environment associated with the STE event, rather than to reproduce the individual short-lived ozone features observed by the lidar. The two datasets are therefore regarded as complementary: the lidar provides high-spatiotemporal-resolution information on local ozone variability, whereas ERA5 provides the dynamically consistent three-dimensional meteorological fields required for diagnosing the tropopause structure and cross-tropopause transport.

Following the approach of Yang et al, we conduct a sensitivity analysis over a domain centered on the Yangbajing ozone lidar site (29°N, 99°E), spanning 25-32°N and 94-104°E, to assess how the choice of PV threshold influences the diagnosed cross-tropopause flux. As shown in Fig. 6, we quantify the changes in cross-tropopause transport on 18-19 October 2017 associated with different PV thresholds within this region. The results indicate that the estimated cross-tropopause flux is highly sensitive to the choice of threshold. For PV thresholds below 3 PVU, both upward and downward transports are relatively large, exhibiting more tropospheric characteristics; for thresholds above 3 PVU, both transports are markedly smaller, consistent with more stratospheric behavior. With increasing PV threshold, the total exchange in both TST and STT decreases. In addition, the magnitudes and temporal evolution of TST and STT suggest that, before and after the onset and recovery of the descent event on 18-19 October 2017, the total cross-tropopause transport over the study region is broadly consistent with mass conservation.

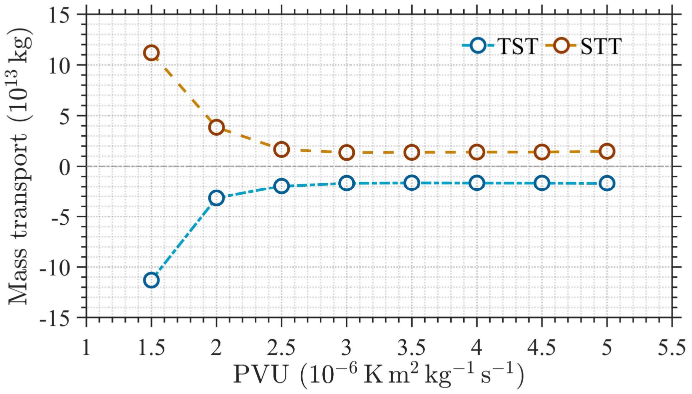

Figure 6: Transport sensitivity to PVU threshold during 18-19 October 2017.

Furthermore, as shown in Fig. 7(a-b), to ensure spatial continuity and robustness of the tropopause definition, we construct two PVU cross-sections from ERA5 in the vicinity of the lidar site: a zonal section along 90-110°E and a meridional section along 24-34°N. These sections show that, in some areas, tropopauses defined using lower PVU thresholds become discontinuous in pressure coordinates. By contrast, the continuity and stability improve markedly for thresholds of 2 PVU and above. Combining the sensitivity results with the cross-section structures, we consider 3 PVU (1 PVU = $10^{-6}\cdot m^2\cdot s^{-1}\cdot kg^{-1}$) to be a reasonable dynamical tropopause threshold for this event (highlighted with an orange line in fig.7(a-b)). It should be noted that the 3-PVU surface is not assumed to represent an exact tropopause altitude with a prescribed absolute accuracy. Rather, uncertainty associated with the dynamical tropopause definition is evaluated through the PV-threshold sensitivity analysis described above. The 3-PVU threshold is therefore adopted as a physically reasonable regional-scale dynamical boundary for this event based on both the sensitivity of the diagnosed transport and the spatial continuity of the corresponding PV surface.

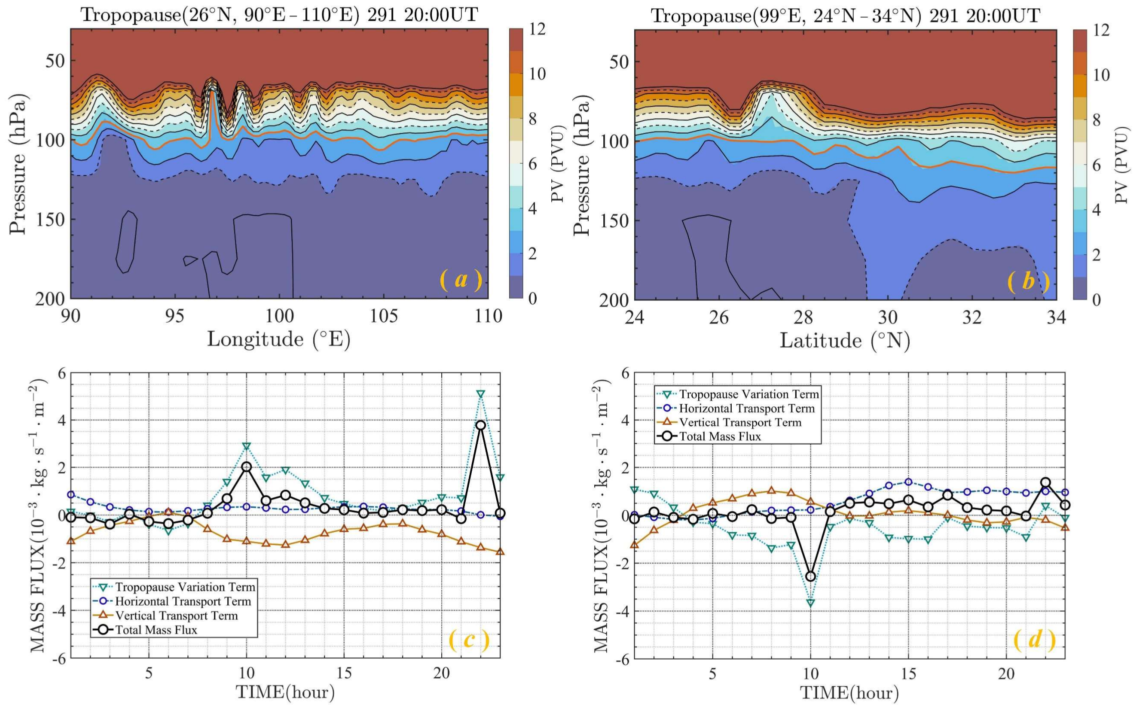

Figure 7: Potential-vorticity structure and cross-tropopause transport over the Tibetan Plateau during 18-19 October 2017. (a) Zonal potential-vorticity cross-section over the Tibetan Plateau region; (b) meridional potential-vorticity cross-section over the Tibetan Plateau region; (c) time evolution of the domain-mean transport components on 18 October; and (d) time evolution of the domain-mean transport components on 19 October.

Fig. 7(c-d) shows the time evolution of the domain mean transport components over 18-19 October 2017, diagnosed from ERA5. The wind fields used in this analysis are obtained from the ERA5 reanalysis, which assimilates a wide range of atmospheric observations and provides observation-constrained, dynamically consistent three-dimensional meteorological fields (Hersbach et al., 2020). Here, the ERA5 wind fields are used to characterize the regional-scale circulation and to provide the dynamical quantities required for the cross-tropopause flux diagnosis, rather than to reproduce the individual short-lived structures resolved by the lidar. The vertical wind contribution remains relatively steady over the two days. The horizontal wind contribution is of comparable magnitude but opposite sign, so that the net flux is controlled to a large extent by variations in the tropopause. It should be stressed that tropopause undulations mainly modify the geometric boundary used in the flux diagnosis and do not, by themselves, generate strong and persistent local transport.

Given the observed tropopause variations, a natural question is whether they were driven by temperature fluctuations in the tropopause region, and in particular whether such temperature changes corresponded to the short-lived, rapid ozone descent events shown in Fig. 4. As discussed above, ERA5 is used here to characterize the larger-scale dynamical evolution of the event, but its hourly output cannot fully resolve the short-lived variability observed by the lidar. Therefore, to examine whether the individual ozone-displacement episodes are accompanied by rapid temperature variations near the tropopause, we use the higher-temporal-resolution temperature profiles retrieved from the 387-nm N_2 Raman lidar signal. As described in Section 2, the USTC Ozone Lidar also recorded the N_2 vibrational Raman backscatter signals at 332 and 387 nm, corresponding to the 308 and 355 nm emission wavelengths, respectively, and these signals exhibit sufficient signal-to-noise ratio over the 14 to 30 km altitude range, as shown in Fig. 8(a). Because 332 nm remains within the ozone absorption band, the 387 nm Raman signal was used to retrieve the temperature profiles. The temperature retrieval, shown in Fig. 8(b), was initialized at 50 km using the temperature from the U.S. Standard Atmosphere 1976 as the upper-boundary reference (U.S. Standard Atmosphere, 1976), and the temperature profile was subsequently retrieved downward from this reference altitude. Comparison with ERA5 at the same times shows that the two temperature profiles are in close agreement. Figure 8(c-d) present the temperature variations retrieved from the 387 nm return over 14.5 to 17 km, where the temperature enhancements at the seven times T0 to T6 correspond closely to those identified in Fig. 4. These results indicate a strong association between the short-lived, rapid ozone descent events and temperature fluctuations in the tropopause region. Moreover, except for T2, all six of the other descent episodes are associated with temperature gradients exceeding 8 K km^{-1}, while T2 still exhibits a pronounced gradient of 4.2 K km^{-1}. They also represent the first detection of these descent features by the USTC Ozone Lidar, together with the first identification of their relationship to tropopause-region temperature variability using lidar-derived temperature profiles.

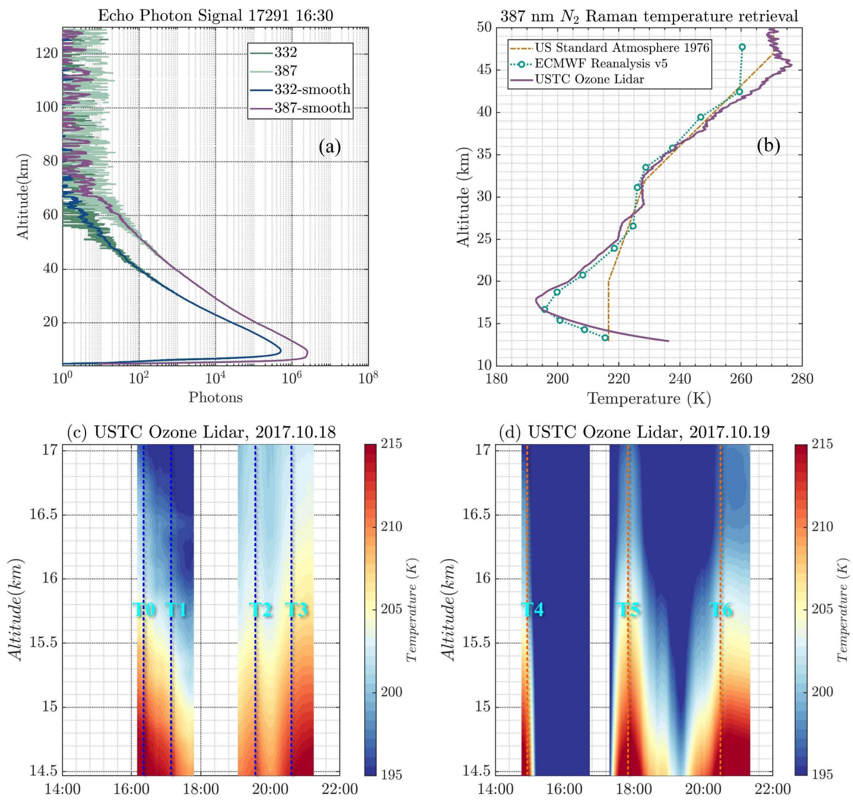

Figure 8: (a) 332 and 387nm echo optical signals received by USTC Ozone Lidar and data smoothing processing; (b) Using the USSA1976 model at a reference point of 50km, the temperature profile obtained by inversion using the 387nm vibrational Raman

signal is compared with that of ERA5; (c) Temperature changes obtained from the inversion on October 18, 2017; (d) Temperature changes obtained from the inversion on October 19, 2017.

Turning back to Fig. 7(c-d), the temporal evolution of the domain-mean flux reveals pronounced stratosphere-to-troposphere transport from 08:00UT to 15:00UT on 18 October and from 21:00UT on 18 October to 03:00UT on 19 October. As the analysis here focuses on the descent event, STT is defined as positive flux. The STE signal begins to recover around 10:00 on 19 October, consistent with the features in Fig. 5a, indicating that the dominant impact of this event is confined to within roughly 24 hours. We also note that, in a domain-mean sense, the onset of the descent signal on 18 October precedes the STE timing inferred at the Yangbajing site (29°N, 99°E) from both the lidar observations and the ERA5-based diagnosis. This apparent lead suggests that the event may have first intensified in a core region away from the site, and then expanded to influence the vicinity of the observation station. To identify the main source region of the event and investigate its dynamical drivers, we further examine the spatial distribution of the cross-tropopause mass flux.

3.3 Spatial Distribution of Mass Fluxes Through the Tropopause

Using Wei's diagnostic framework together with ERA5 meteorological fields, we quantify the cross-tropopause mass exchange flux during 13:00UT-18:00UT on 18 October. The flux is decomposed into contributions associated with tropopause motion, horizontal advection, and vertical motion, and we map the 6-hour mean of the instantaneous mass flux over this period (Fig.9). The red hexagon marks the location of the Yangbajing ozone lidar site. As shown in Fig.9, the horizontal transport term exhibits a spatial distribution highly consistent with that of the total flux, with a comparable magnitude. This suggests that the spatial structure of the flux during this STE event was controlled mainly by horizontal transport. However, the flux estimates shown earlier in Fig. 7(a-b) indicate that the actual downward mass transport was induced by the tropopause motion term. Moreover, Figure 9(c) further indicates that downward transport associated with the vertical transport term was also present at the Yangbajing lidar site. This behavior is consistent with the dynamical picture of tropopause folding (Sprenger et al., 2001; Škerlak et al., 2015). The regional PV structure indicates a tropopause-folding system over approximately 25-28°N, 95-99°E, characterized by a pronounced deformation and downward intrusion of stratospheric high-PV air toward the troposphere. The corresponding structure can also be identified in the PV cross-section near 26°N in Fig. 7(a), and its spatial extent closely overlaps the region of enhanced cross-tropopause mass flux shown in Fig. 9. We note that the shorter-timescale oscillations of the tropopause observed during the evolution of the event do not contradict this regional folding interpretation. Tropopause folds developing in strongly sheared jet–front environments can be accompanied by inertia-gravity waves, wave breaking, and related instabilities, which further modulate and locally deform the tropopause and can contribute to irreversible mixing and STE (Cho et al., 1999; Bertin et al., 2001; Stohl et al., 2003). We therefore interpret the observed evolution as a regional tropopause-folding system accompanied and modulated by shorter-timescale wave-related tropopause variability.

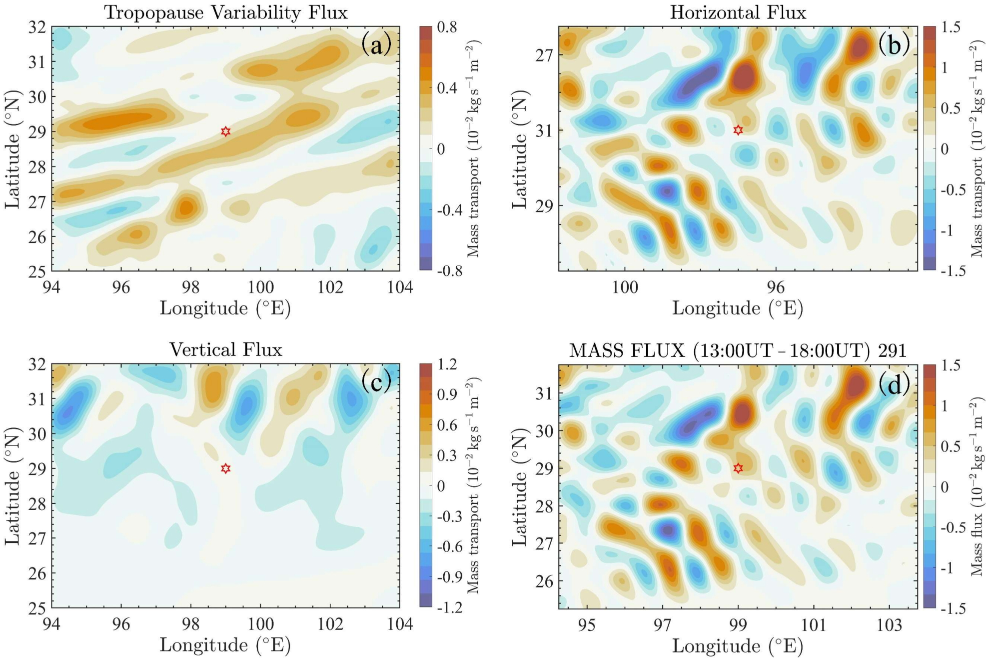

Figure 9: Spatial distributions of the cross-tropopause mass-flux components diagnosed using Wei's formulation and ERA5 meteorological fields during 13:00-18:00 on 18 October 2017. Each panel shows the 6-h mean of the instantaneous mass flux: (a) Transport contribution from tropopause motion; (b) Horizontal transport term; (c) Vertical transport term; (d) Total cross-tropopause mass flux. The red asterisk marks the location of the USTC Ozone Lidar at Yangbajing (29°N, 99°E).

As shown in Fig. 10, we use ERA5 meteorological fields together with Wei's diagnostic to derive the spatiotemporal evolution of cross-tropopause mass flux over the study region during 18-19 October 2017. Eulerian diagnostics formulated in pressure coordinates can be affected by numerical cancellation among individually large terms, potentially introducing substantial uncertainty into estimates of cross-tropopause fluxes (Wirth, 1995; Wirth and Egger, 1999). Lagrangian approaches, such as those developed and applied in previous studies (Wernli, 2002; Škerlak et al., 2014), provide an alternative that is generally less susceptible to this numerical-cancellation problem, particularly for global or large-domain analyses. However, because the present study focuses on the regional evolution of a specific STE event rather than on global-scale transport, we retained Wei's diagnostic framework but reformulated it in potential-vorticity coordinates. The corresponding results are presented in Fig. 10. Although this coordinate transformation does not eliminate all sources of uncertainty, it alleviates the numerical sensitivity and reduces part of the noise associated with cancellation among large terms. Each panel presents the 6-hour mean of the instantaneous mass flux for the corresponding interval. From Fig. 10(a-e), the tropopause-folding structure over 25-28°N, 95-99°E evolves markedly with time, and the associated mass flux field exhibits pronounced temporal non-stationarity and spatial heterogeneity. This sector lies along the southeastern flank of the Tibetan Plateau, within the transition zone between the entrance and exit regions of the upper-tropospheric jet, where strong shear and dynamical disturbances favor tropopause deformation, folding, and associated wave activity. Notably, the clearly identifiable folding band transitions from an approximately quasi-parallel, banded morphology in Fig.10(a-b) to a meridionally offset, interleaving structure in Fig. 10(g-h), suggesting a shift in the folding process from a stage modulated by near-linear wave perturbations towards a more strongly nonlinear breaking regime, possibly associated with inertial gravity waves induced by tropopause folding and their subsequent breaking. Given the fixed station location, the lidar measurements do not continuously sample the core of the tropopause fold, but more often reflect the downstream evolution and lateral modulation of the folding system (Shangguan et al., 2019; Zhang et al., 2024).

We offer the following conceptual interpretation of the dynamics. During the phase in Fig. 10(a-b), PV anomalies near the tropopause are characterized by quasi-parallel PV contours, a relatively weak meridional gradient, and limited vertical extension. This structure suggests that folding is primarily modulated by disturbances, such as planetary waves and inertial gravity waves, superimposed on the shear environment of the upper-tropospheric jet (McIntyre et al., 1983). In this stage, the lidar site (29°N, 99°E) lies on the northern flank of the folding band, within a wave-dominated sector that mainly reflects perturbations associated with tropopause undulations and PV field oscillations, while the net cross-tropopause transport remains limited. In Fig. 10(c-f), as instability strengthens in the jet-exit region, the PV gradient across the folding band sharpens markedly. An ascending branch develops on the southern side of the fold, whereas a quasi-stationary descending branch forms on the northern side near the lidar site. The site then becomes intermittently aligned with the downstream transport pathway of the PV anomaly, indicating a transition from a fold evident in morphology to one that enables effective transport (Sprenger et al., 2003). In Fig. 10(g-h), the fold exhibits clear PV tongue breakup and meridional displacement. The sawtooth-like offsets likely reflect wave breaking or nonlinear PV mixing (McIntyre et al., 1983; McIntyre et al., 1984). At this stage, ascent-descent dipoles occur more frequently on smaller spatial scales, and the vertical circulation becomes shorter-lived and more localized. The previously coherent descending conduit weakens and becomes increasingly intermittent (Stohl et al., 2003). In the vicinity of the site, this fragmented circulation and enhanced mixing reduce sustained stratosphere-to-troposphere transport (STT), manifesting as a weakened or discontinuous downward flux. In addition, the ascending branch structure to the south of the site can further interrupt the local descent pathway.

Taken together, these results indicate that the short-lived, rapid ozone descent observed during this STE event was associated not only with temperature variations, but also that the onset and recovery of the event as a whole were modulated by tropopause folding and gravity waves over the region 25-28°N, 95-99°E.

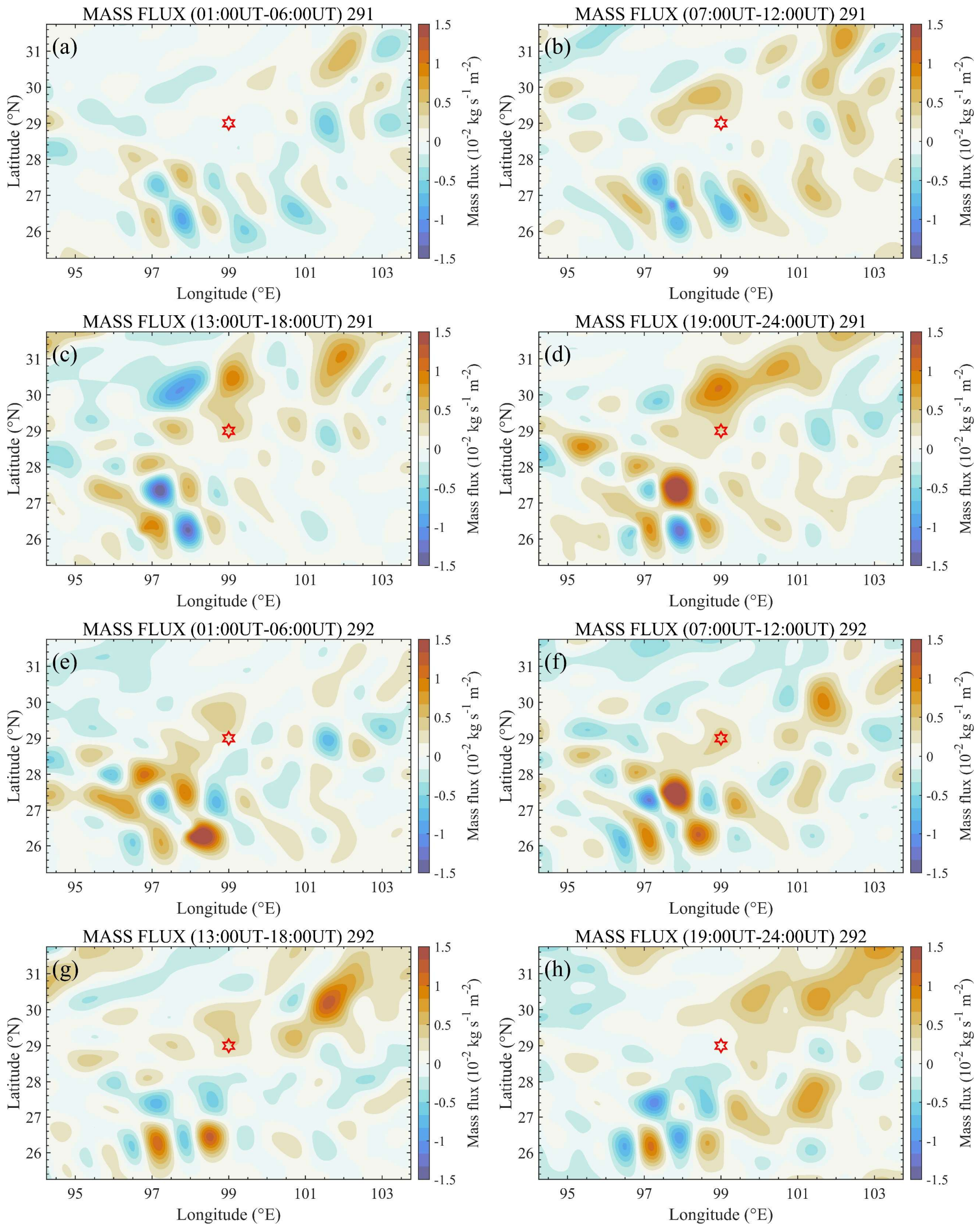

435 **Figure 10: Spatiotemporal evolution of the cross-tropopause mass flux during 18-19 October 2017, diagnosed using Wei's formulation and ERA5 meteorological fields. Each panel shows the 6-h mean of the instantaneous cross-tropopause mass flux for the corresponding time interval. The red asterisk marks the location of the USTC Ozone Lidar at Yangbajing (29°N, 99°E).**

3.4 Cross-tropopause ozone flux estimation based on lidar observations

Building on the mass-flux diagnostics, we further estimate the cross-tropopause ozone flux by incorporating ozone profiles from the USTC Ozone Lidar. Specifically, we use the lidar-retrieved vertical profiles of ozone number density to characterize ozone abundance in the troposphere and stratosphere and, in combination with the diagnosed cross-tropopause mass flux, to quantify ozone exchange across a layer extending several kilometers above and below the tropopause.

To ensure the robustness of the calculation, we assume that the ozone number densities measured at the lidar site (29°N, 99°E) are representative of the mean ozone level within 28.75-29.25°N and 98.75-99.25°E. Consistently, the mass flux is diagnosed from ERA5 gridded fields over the same spatial domain. Following Cui et al. (2004), the lidar-derived, vertically varying ozone mixing-ratio profiles are integrated over the 3-km layers immediately below and above the tropopause to obtain representative layer-mean mixing ratios. Consequently, the measured vertical ozone gradients within these layers are retained in the calculation rather than being replaced by a vertically uniform ozone concentration.

$$F_q = M_{up}\frac{\int_{p_{tropopause-3}}^{p_{tropopause}} q(p)dp}{\int_{p_{tropopause-3}}^{p_{tropopause}} dp} + M_{down}\frac{\int_{p_{tropopause}}^{p_{tropopause+3}} q(p)dp}{\int_{p_{tropopause}}^{p_{tropopause+}} dp}, \quad (3)$$

In the equation, $q(p)$ represents the uniform mixing ratio of ozone at pressure p, M_{up} denotes the upward flux of substances through the tropopause, and M_{down} denotes the downward flux of substances. Positive and negative values indicate locations above and below the tropopause, respectively. Thus, the observed vertical variation of ozone within the 3-km layers above and below the tropopause is retained in the integration rather than assuming a vertically uniform ozone abundance. The two integral terms represent the pressure-weighted layer-mean ozone mixing ratios on the tropospheric and stratospheric sides of the tropopause, respectively.

The instantaneous cross-tropopause ozone flux diagnosed at the Yangbajing lidar site for 18-19 October 2017 is shown in Fig. 11. A clear STE-related ozone descent signal is evident from 13:00 on 18 October to 12:00 on 19 October, manifested as a positive ozone flux from the stratosphere to the troposphere. In contrast, Aura satellite sampling near the site is temporally sparse. MLS typically overpasses the vicinity of Yangbajing only twice per day, whereas OMI provides at most one pass per day, which largely explains the relatively low temporal resolution of the satellite products. For 18-19 October, MLS provides three nearby footprints at (29.66°N, 98.27°E), (25.22°N, 105.20°E), and (29.66°N, 95.52°E) (red hexagons in Fig. 11). The first and third footprints are closest to the Yangbajing site, and the ozone fluxes inferred from MLS there agree well with the ERA5 estimates. By contrast, the second footprint is displaced substantially in longitude and lies outside the Tibetan Plateau, and its inferred ozone flux deviates more strongly from both the ERA5 and lidar results. Overall, the ozone flux derived from the USTC Ozone Lidar measured profiles is broadly consistent with the ERA5-driven ozone flux. More specifically, on 18 October, the lidar observations mainly capture the intensification phase and yield slightly larger diagnosed fluxes than ERA5, whereas on 19 October, during the recovery phase, the two estimates closely agree.

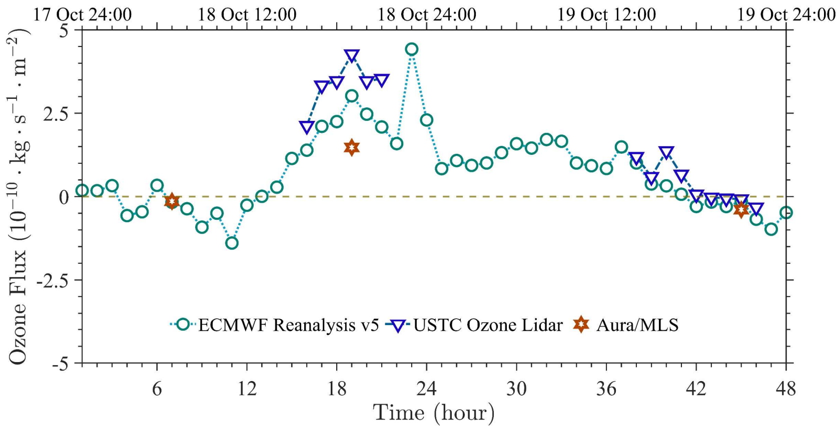

Fig. 11. Instantaneous cross-tropopause ozone flux during 18-19 October 2017.

In this study, we present an initial detection and analysis of a stratosphere–troposphere exchange (STE) event captured by ozone lidar observations. The ozone flux associated with stratosphere-to-troposphere transport derived from the USTC Ozone Lidar exhibits an instantaneous peak of approximately $3\text{-}4 \cdot 10^{-10} \cdot kg \cdot s^{-1} \cdot m^{-2}$, slightly exceeding the corresponding estimate derived from ERA5 for the same period. Despite this difference, the overall agreement between the lidar-derived and ERA5-derived ozone fluxes supports the robustness of the flux-calculation framework. Although ozone lidar provides ozone concentration measurements with high spatial and temporal resolution, the lack of time-continuous in situ wind observations necessitates the use of ERA5 wind fields at 1-hour resolution in the flux diagnosis. Despite this limitation, our analysis demonstrates that ozone-profiling lidar can not only resolve the fine vertical structure of ozone but also, when combined with wind information, enable quantitative observation and flux estimation of STE-related downward ozone transport, thereby broadening the potential of lidar for studies of coupled atmospheric composition and dynamics.

4 Conclusion

This study uses vertical profiles of ozone density observed by our mobile differential absorption ozone lidar (USTC Ozone Lidar) located at Yangbajing, Tibet (29°N, 99°E). The system provides synchronous observations of tropospheric and stratospheric ozone over 5-50 km, offering high-spatiotemporal-resolution profile evidence for STE studies over the Tibetan Plateau. By combining 30-min signal accumulation with a moving-window procedure, the dataset maintains a high effective temporal sampling while ensuring an adequate signal-to-noise ratio and showing strong consistency with ECMWF Reanalysis v5 (ERA5) and independent satellite observations.

To corroborate the STE-related ozone descent event identified from the lidar retrievals on 18-19 October 2017, ERA5 global reanalysis was used as an independent constraint. Near the tropopause, the ozone number densities observed by the USTC Ozone Lidar agree closely with ERA5 in both magnitude and temporal evolution, lending confidence to the event identification and the subsequent quantitative diagnostics. For the rapid ozone descent features resolved by the lidar, temperature profiles retrieved from the 387-nm N_2 vibrational Raman return reveal a strong correspondence with temperature fluctuations in the tropopause region. In six of the seven identified descent episodes, the associated temperature gradient exceeds 8 K km^{-1}, and even in the remaining case the gradient still reaches 4.2 K km^{-1}. These results represent the first detection of such rapid descent features by the USTC Ozone Lidar, together with the first identification of their close relationship to tropopause-region temperature variability using lidar-derived temperature profiles. In addition, the ozone descent observed at Yangbajing generally lags the broader descent over the study region (25-32°N, 94-104°E). The spatial distribution of cross-tropopause mass flux was diagnosed using the Wei formulation, with the PV-threshold sensitivity analysis supporting 3 PVU as a physically reasonable dynamical tropopause threshold for this event. The diagnosed flux fields further suggest that this STE event was closely linked to tropopause folding within the study region (25-32°N, 94-104°E), with the ozone variability observed at the lidar site modulated by gravity waves associated with the evolving fold.

Building on the mass-flux diagnosis, we directly incorporate lidar-measured ozone profiles into a cross-tropopause ozone-flux framework to quantify the downward ozone flux and validate the estimates against ERA5-driven results and Aura/MLS observations. The results show that the instantaneous peak ozone flux associated with stratosphere-to-troposphere transport, measured by the USTC Ozone Lidar, is approximately $3\text{-}4 \cdot 10^{-10} \cdot kg \cdot s^{-1} \cdot m^{-2}$, slightly exceeding the corresponding ERA5-derived estimate for the same period. Because time-continuous in situ wind measurements are not available, the flux calculation still relies on ERA5 wind fields. Even with this limitation, the results demonstrate that ozone-profiling lidar can resolve fine-scale vertical ozone structures and, when combined with wind information and dynamical diagnostics, contribute to the quantitative assessment of STE-related ozone transport and cross-tropopause ozone fluxes. Looking ahead, we will further develop and deploy a high-accuracy, high-temporal-resolution vertical wind profiling lidar to strengthen observations of coupled composition-dynamics processes over Tibet and to extend the utility of ozone lidar in such studies.

Code and data availability

Data and code underlying the results presented in this paper are not publicly available at this time but may be obtained from the authors upon reasonable request.

Author contributions

Conceptualization, R.D. and X.F.; methodology, R.D.; validation, R.D., C.Y. and X.F.; formal analysis, C.Y.; writing-original draft preparation, R.D.; writing-review and editing, T.L.; funding acquisition, C.Y. All authors have read and agreed to the published version of the manuscript.

Competing interests

The authors declare no conflicts of interest

Acknowledgements

We thank all other members in team for their contribution to the system installation. We also thank Dan Chen, Yun Bi, Xianhang Chen, and the other colleagues and students who provided valuable assistance. We acknowledge for the data resources from " National Space Science Data Center, National Science & Technology Infrastructure of China. (https://www.nssdc.ac.cn)". We acknowledge for the data provider University of Science and Technology of China. The Aura/MLS data is downloaded from https://search.earthdata.nasa.gov/search.

Financial support

National Natural Science Foundation of China (grant nos.42130203 and 41974177); National Key Research and Development Program of China (2022YFF0503703); B-type Strategic Priority Program of the Chinese Academy of Sciences (XDB41000000).

References

Ancellet, G., Pelon, J., Beekmann, M., Papayannis, A., and Mégie, G.: Ground-Based Lidar Studies of Ozone Exchanges Between the Stratosphere and the Troposphere, J. Geophys. Res., 96, 22401–22421, 1991.

Baray, J. L., Courcoux, Y., Keckhut, P., Portafaix, T., Tulet, P., Cammas, J. P., ... & Delmas, R. (2013). Maïdo observatory: a new high-altitude station facility at Reunion Island (21° S, 55° E) for long-term atmospheric remote sensing and in situ measurements. Atmospheric Measurement Techniques, 6(10), 2865-2877.

Bertin, F., Campistron, B., Caccia, J. L., & Wilson, R. (2001, August). Mixing processes in a tropopause folding observed by a network of ST radar and lidar. In Annales Geophysicae (Vol. 19, No. 8, pp. 953-963). Göttingen, Germany: Copernicus Publications.

Browell, E. V., Ismail, S., & Shipley, S. T. (1985). Ultraviolet DIAL measurements of O3 profiles in regions of spatially inhomogeneous aerosols. Applied Optics, 24(17), 2827-2836.

Boggess, A., & Narcowich, F. J. (2009). A first course in wavelets with Fourier analysis. John Wiley & Sons.

CHEN Bin, XU Xiang-De, BIAN Jian-Chun, SHI Xiao-Hui. Irreversible stratosphere-troposphere mass exchange characteristics over the Asian summer monsoon region[J]. Chinese Journal of Geophysics (in Chinese), 2010, 53(5): 1050-1059.

Chen, C., Tian, W. S., Tian, H. Y., Huo, Y., Shu, J., Xie, F., ... & Wan, X. W. (2012). Vertical distribution of ozone and stratosphere-troposphere exchanges on the northeastern side of Tibetan Plateau. Plateau Meteorology, 31(2), 295-303.

Chen Hongbin, Bian Jianchun, Lü Daren. Advances and prospects in the study of stratosphere-troposphere exchange. Chinese Journal of Atmospheric Sciences (in Chinese), 2006, 30(5): 813-820.

Cho, J. Y., Newell, R. E., Bui, T. P., Browell, E. V., Fenn, M. A., Mahoney, M. J., ... & Thompson, A. M. (1999). Observations of convective and dynamical instabilities in tropopause folds and their contribution to stratosphere - troposphere exchange. Journal of Geophysical Research: Atmospheres, 104(D17), 21549-21568.

Cui, H., Zhao, C., Qin, Y., Zheng, X., Zheng, Y., Chan, C. Y., & Chan, L. Y. (2004). An estimation of ozone flux in a stratosphere-troposphere exchange event. Chinese Science Bulletin, 49(2), 167-174.

Duan, A. M., & Wu, G. X. (2005). Role of the Tibetan Plateau thermal forcing in the summer climate patterns over subtropical Asia. Climate Dynamics, 24(7), 793-807.

Duchnowski, R., & Wyszkowska, P. (2025). Laser scanning data processed using Msplit estimation and sliding window algorithm. Reports on Geodesy and Geoinformatics, 120(1), 67-74.

Eisele, H., Scheel, H. E., Sladkovic, R., & Trickl, T. (1999). High-resolution lidar measurements of stratosphere–troposphere exchange. Journal of the Atmospheric Sciences, 56(2), 319-330.

Fang, H., & Huang, D. (2004). Lidar signal de-noising based on wavelet trimmed thresholding technique. Chinese Optics Letters, 2(1), 1-3.

Fang, X., Li, T., Ban, C., Wu, Z., Li, J., Li, F., ... & Tian, B. (2019). A mobile differential absorption lidar for simultaneous observations of tropospheric and stratospheric ozone over Tibet. Optics Express, 27(4), 4126-4139.

Gettelman, A., Salby, M. L., & Sassi, F. (2002). Distribution and influence of convection in the tropical tropopause region. Journal of Geophysical Research: Atmospheres, 107(D10), ACL-6.

Gimmestad, G. G. (2005). Differential-Absorption Lidar for Ozone and Industrial Emissions. In C. Weitkamp (Ed.), Lidar: Range-Resolved Optical Remote Sensing of the Atmosphere, Springer Series in Optical Sciences, Vol. 102, pp. 187–212. Springer.

Godin-Beekmann, S., Porteneuve, J., & Garnier, A. (2003). Systematic DIAL lidar monitoring of the stratospheric ozone vertical distribution at Observatoire de Haute-Provence (43.92 N, 5.71 E). Journal of Environmental Monitoring, 5(1), 57-67.

Hansen, G., Bramstedt, K., Rozanov, V., Weber, M., & Burrows, J. P. (2003, August). Validation of GOME ozone profiles by means of the ALOMAR ozone lidar. In Annales Geophysicae, 21(8), 1879-1886. Göttingen, Germany: Copernicus Publications.

Hersbach, H., Bell, B., Berrisford, P., Hirahara, S., Horányi, A., Muñoz - Sabater, J., ... & Thépaut, J. N. (2020). The ERA5 global reanalysis. Quarterly journal of the royal meteorological society, 146(730), 1999-2049.

Holton, J. R., Haynes, P. H., McIntyre, M. E., Douglass, A. R., Rood, R. B., & Pfister, L. (1995). Stratosphere-troposphere exchange. Reviews of Geophysics, 33(4), 403-439.

Kuang, S., Newchurch, M. J., Burris, J., Wang, L., Knupp, K., & Huang, G. (2012). Stratosphere-to-troposphere transport revealed by ground-based lidar and ozonesonde at a midlatitude site. Journal of Geophysical Research: Atmospheres, 117(D18).

Kourtidis, K., Zerefos, C., Rapsomanikis, S., Simeonov, V., Balis, D., Perros, P. E., ... & Drakou, R. (2002). Regional levels of ozone in the troposphere over eastern Mediterranean. Journal of Geophysical Research: Atmospheres, 107(D18), PAU-7.

Kovalev, V. A., & Eichinger, W. E. (2004). Elastic lidar: theory, practice, and analysis methods. John Wiley & Sons.

Kovalev, V. A., & Bristow, M. P. (1996). Compensational three-wavelength differential-absorption lidar technique for reducing the influence of differential scattering on ozone-concentration measurements. Applied optics, 35(24), 4790-4797.

Langford, A. O., Masters, C. D., Proffitt, M. H., Hsie, E.-Y., and Tuck, A. F.: Ozone measurements in a tropopause fold associated with a cut-off low system, Geophys. Res. Lett., 23, 2501–2504, 1996.

Lelieveld, J., & Dentener, F. J. (2000). What controls tropospheric ozone? Journal of Geophysical Research: Atmospheres, 105(D3), 3531-3551.

Liu, X., Bhartia, P. K., Chance, K., Spurr, R. J. D., & Kurosu, T. P. (2010). Ozone profile retrievals from the Ozone Monitoring Instrument. Atmospheric Chemistry and Physics, 10(5), 2521-2537.

McDermid, I. S., Haner, D. A., Kleiman, M. M., Walsh, T. D., & White, M. L. (1991). Differential absorption lidar systems for tropospheric and stratospheric ozone measurements. Optical Engineering, 30(1), 22-30.

McGee, T. J., Gross, M., Ferrare, R., Heaps, R., and Singh, U.: Raman DIAL measurements of stratospheric ozone in the presence of volcanic aerosols, Geophys. Res. Lett., 20, 955–958 1993.

McIntyre, M. E., & Palmer, T. N. (1983). Breaking planetary waves in the stratosphere. Nature, 305(5935), 593-600.

McIntyre, M. E., & Palmer, T. N. (1984). The “surf zone” in the stratosphere. Journal of Atmospheric and Terrestrial Physics, 46(9), 825-849.

Olsen, M. A., Schoeberl, M. R., & Douglass, A. R. (2004). Stratosphere-troposphere exchange of mass and ozone. Journal of Geophysical Research: Atmospheres, 109(D24).

Papayannis, A. D., Porteneuve, J., Balis, D., Zerefos, C., & Galani, E. (1999). Design of a new DIAL system for tropospheric and lower stratospheric ozone monitoring in Northern Greece. Physics and Chemistry of the Earth, Part C: Solar, Terrestrial & Planetary Science, 24(5), 439-442.

Randel, W. J., & Park, M. (2006). Deep convective influence on the Asian summer monsoon anticyclone and associated tracer variability observed with Atmospheric Infrared Sounder (AIRS). Journal of Geophysical Research: Atmospheres, 111(D12).

Randel, W. J., Park, M., Emmons, L., Kinnison, D., Bernath, P., Walker, K. A., ... & Pumphrey, H. (2010). Asian monsoon transport of pollution to the stratosphere. Science, 328(5978), 611-613.

Reiter, E. R. (1975). Stratospheric-tropospheric exchange processes. Reviews of Geophysics, 13(4), 459-474.

Schoeberl, M. R., Douglass, A. R., Hilsenrath, E., Bhartia, P. K., Beer, R., Waters, J. W., ... & DeCola, P. (2006). Overview of the EOS Aura mission. IEEE Transactions on Geoscience and Remote Sensing, 44(5), 1066-1074.

Shangguan, M., Wang, W., & Jin, S. (2019). Variability of temperature and ozone in the upper troposphere and lower stratosphere from multi-satellite observations and reanalysis data. Atmospheric Chemistry and Physics, 19(10), 6659-6679.

Škerlak, B., Sprenger, M., Pfahl, S., Tyrlis, E., & Wernli, H. (2015). Tropopause folds in ERA-Interim: Global climatology and relation to extreme weather events. Journal of Geophysical Research: Atmospheres, 120(10), 4860-4877.

Škerlak, B., Sprenger, M., & Wernli, H. (2014). A global climatology of stratosphere-troposphere exchange using the ERA-Interim data set from 1979 to 2011. Atmospheric Chemistry and Physics, 14(2), 913-937.

Sprenger, M., Croci Maspoli, M., & Wernli, H. (2003). Tropopause folds and cross-tropopause exchange: A global investigation based upon ECMWF analyses for the time period March 2000 to February 2001. Journal of Geophysical Research: Atmospheres, 108(D12).

Standard, U. S. (1976). Atmosphere. National Oceanic and Atmospheric Administration.

Stohl, A., Bonasoni, P., Cristofanelli, P., Collins, W., Feichter, J., Frank, A., ... & Zerefos, C. (2003). Stratosphere-troposphere exchange: A review, and what we have learned from STACCATO. Journal of Geophysical Research: Atmospheres, 108(D12).

Tian, W., Chipperfield, M., & Huang, Q. (2008). Effects of the Tibetan Plateau on total column ozone distribution. Tellus B: Chemical and Physical Meteorology, 60(4), 622-635.

Trickl, T., Vogelmann, H., Ries, L., & Sprenger, M. (2020). Very high stratospheric influence observed in the free troposphere over the northern Alps–just a local phenomenon?. Atmospheric Chemistry and Physics, 20(1), 243-266.

Waters, J. W., Froidevaux, L., Harwood, R. S., Jarnot, R. F., Pickett, H. M., Read, W. G., ... & Walch, M. J. (2006). The earth observing system microwave limb sounder (EOS MLS) on the Aura satellite. IEEE transactions on geoscience and remote sensing, 44(5), 1075-1092.

Wernli, H., & Bourqui, M. (2002). A Lagrangian “1 - year climatology” of (deep) cross - tropopause exchange in the extratropical Northern Hemisphere. Journal of Geophysical Research: Atmospheres, 107(D2), ACL-13.

Wei, M. Y. (1987). A new formulation of the exchange of mass and trace constituents between the stratosphere and troposphere. Journal of Atmospheric Sciences, 44(20), 3079-3086.

Wirth, V. (1995). Comments onA new formulation of the exchange of mass and trace constituents between the... Journal of the atmospheric sciences, 52(13), 2491.

Wirth, V., & Egger, J. (1999). Diagnosing extratropical synoptic-scale stratosphere-troposphere exchange: A case study. Quarterly Journal of the Royal Meteorological Society, 125(554), 635-655.

Yang Jian, Lv Daren. A Simulation Study of Stratosphere-Troposphere Exchange due to Cut-off-low over Eastern Asia. Chinese Journal of Atmospheric Sciences (in Chinese), 2003, 27(6): 1031-1044.

YANG Jian, LU Da-Ren. Diagnosed Seasonal Variation of Stratosphere-Troposphere Exchange in the Northern Hemisphere by 2000 Data. Chinese Journal of Atmospheric Sciences (in Chinese), 2004, 28(2): 294-300.

Yin, S., & Wang, W. (2006). Denoising lidar signal by combining wavelet improved threshold with wavelet domain spatial filtering. Chinese Optics Letters, 4(12), 694-696.

Zhang, M., Tian, W., Chen, L., & Lü, D. (2010). Cross-tropopause mass exchange associated with a tropopause fold event over the northeastern Tibetan Plateau. Advances in Atmospheric Sciences, 27(6), 1344-1360.

Zhang, Y., Huang, Q., Guo, K., Wang, M., Liao, H., Chou, Y., & He, X. (2024). Tropopause folds over the Tibetan Plateau and their impact on water vapor in the upper troposphere-lower stratosphere. Climate Dynamics, 62(2), 1423-1437.

Zhou, S., & Zhang, R. (2005). Decadal variations of temperature and geopotential height over the Tibetan Plateau and their relations with Tibet ozone depletion. Geophysical Research Letters, 32(18).